Redox Biology 73 (2024) 103175

Contents lists available at ScienceDirect

Redox Biology

journal homepage: www.elsevier.com/locate/redox

circMIRIAF aggravates myocardial ischemia-reperfusion injury via targeting miR-544/WDR12 axis

Lianhong Yin [a], Lili Li [d], Meng Gao [a], Yan Qi [a], Lina Xu [a,**], Jinyong Peng [a,b,c,*]

[a] Department of Pharmaceutical Analysis, Dalian Medical University, Western 9 Lvshunnan Road, Dalian, 116044, China
[b] College of Pharmacy, Hubei University of Chinese Medicine, Wuhan, 430065, China
[c] Hubei Shizhen Laboratory, Wuhan, 430065, China
[d] College of Pharmacy, Anhui University of Chinese Medicine, Hefei, 230012, China

ARTICLE INFO

Keywords:
Myocardial ischemia-reperfusion injury
circMIRIAF
miR-544
WDR12
Oxidative stress
Inflammation

ABSTRACT

Exploring and discovering novel circRNAs is one of the ways to develop innovative drugs for the diagnosis and treatment of myocardial ischemia-reperfusion injury (MI/RI). In the work, some dysregulated circRNAs were found by microarray screening analysis in AC16 cells, and hsa_circRNA_104852 named circMIRIAF was screened, which was up-regulated in AC16 cells damaged by hypoxia-reoxygenation injury (H/RI). The comprehensive analysis of ceRNA network revealed the potential relationship of circMIRIAF/miR-544/WDR12. Then, the results of interaction research confirmed that circMIRIAF acted as sponge of miR-544 to positively regulate WDR12 protein expression. Further, the validation results indicate that miR-544 silencing increased the expression of WDR12, and WDR12 activated Notch1 signal to aggravate H/RI of AC16 cells and MI/RI of mice via regulating oxidative stress and inflammation. Furthermore, silencing circMIRIAF caused the decreased circMIRIAF levels and the increased miR-544 levels in cardiomyocytes, while excessive miR-544 inhibited WDR12 expression to alleviate the disorder. On the contrary, excessive circMIRIAF increased WDR12 expression by adsorbing miR-544 to exacerbate H/RI in AC16 cells. In addition, circMIRIAF siRNA reversed the aggravation of H/RI in cells caused by WDR12 overexpression. Overall, circMIRIAF can serve as a drug target or treating MI/RI, and circMIRIAF could sponge miR-544 and enhance WDR12 expression to aggravate MI/RI, which may provide a novel therapeutic strategy for MI/RI treatment.

1. Introduction

Cardiovascular disease has become one of the leading causes of death in the world. The clinical therapy of cardiovascular disease is mainly surgical and drug treatment [1,2], in which surgical treatment can achieve rapid recovery of ischemic myocardium blood supply [3–6]. However, sudden process of blood supply can increase blood volume in collateral circulation, and the revascularization will lead to the activation of myocardial ischemia-reperfusion injury (MI/RI), which accounts for 50% of the area of myocardial infarction [7–10]. MI/RI is a key factor to affect the therapeutic effect of coronary heart disease, and its pathogenesis is complex [11,12]. MI/RI can cause inflammatory response to damage viable tissue around the infarct [13], as well as destroy the mitochondrial membrane potential, leading to the formation of reactive oxygen species (ROS) [14–16]. There are various methods used in clinical practice to treat MI/RI, including anti-inflammatory, antioxidant, ischemic preconditioning and drug preconditioning [17]. Administration of vitamin C and vitamin E in patients after coronary artery surgery may significantly reduce MI/RI through antioxidant stress [18]. However, many anti-inflammatory and antioxidant drugs are limited by pharmacokinetics and other factors. Therefore, more researches are urgently needed to fully understand the molecular basis of

Abbreviations: MI/RI, Myocardial ischemia-reperfusion injury; H/RI, hypoxia-reoxygenation injury; SOD, superoxide dismutase; ROS, reactive oxygen species; LDH, lactate dehydrogenase; CK-MB, creatine kinase isoenzyme; cTnI, cardioac troponin I; ECG, electrocardiogram; Hes1, hairy and enhancer of split 1; Hey1, YRPW motif 1; GCLC, glutamate-cysteine ligase catalytic subunit; NOX4, NADPH oxidase 4; Nrf2, nuclear erythroid factor 2-reated factor 2; NF-κB, nuclear factor-kappa B; TNF-α, tumor necrosis factor-α; IL-1β, interleukin-1β; IL-6, interleukin-6; ICAM-1, intercellular cell adhesion molecule-1; PTEN, phosphatase and tensin homolog deleted on chromosome ten; GSH, glutathione.

* Corresponding author. College of Pharmacy, Dalian Medical University Dalian, China.
** Corresponding author. Department of Pharmaceutical Analysis, Dalian Medical University, Western 9 Lvshunnan Road, Dalian, 116044, China.
E-mail addresses: xulina627@163.com (L. Xu), jinyongpeng2005@163.com (J. Peng).

https://doi.org/10.1016/j.redox.2024.103175
Received 2 April 2024; Received in revised form 26 April 2024; Accepted 29 April 2024
Available online 5 May 2024

the disease, identify drug targets to treat MI/RI via adjusting inflammation and oxidative stress, develop therapeutic drugs, and formulate treatment strategies.

Circular RNAs (circRNAs) are a class of non-coding RNA molecules characterized by covalently closed loop structures without 5′ terminal cap and 3′ terminal poly A tail [19]. They play critical roles in a variety of biological processes, such as modulating parental gene expression, regulating RNA-protein interactions, sequestering proteins, and functioning as microRNA sponges [20]. circRNAs are rich in miRNA binding sites, which can act as miRNA sponge to adsorb miRNA to reduce the inhibitory effector of miRNA on its target gene expression [21,22]. Some studies have shown that circRNAs play important roles in MI/RI via ceRNA mechanism [23,24]. For example, circRNA NCX1 can act as an endogenous miR-133a-3p sponge to promote cardiomyocyte apoptosis [25], circANXA2 can promote cardiomyocyte apoptosis in MI/RI by inhibiting miR-133 expression [26], circRNA TLK1 can aggravate MI/RI by inhibiting miR-214 [27]. Some compounds have been used to treat MI/RI by regulating circRNAs. Sevoflurane exerts protection against MI/RI through circRNA PAN3/miRNA-29b-3p/stromal cell-derived factor 4 axis [28]. Salvianolic acid B protects cardiomyocytes from MI/RI by mediating circTRRAP/miR-214-3p/SOX6 axis [29]. Salidroside inhibits apoptosis and autophagy of cardiomyocyte by regulating hsa_ circ_0000064 in MI/RI [30]. Therefore, it is of great significance to explore new circRNAs and elucidate the molecular mechanisms for the development of innovative drugs to treat MI/RI.

Endogenous Notch1 is essential to promote cardiomyocyte survival, inhibit myocardial fibrosis and maintain cardiac function, which can also regulate cell development, proliferation, differentiation and regeneration [31–34]. Activating Notch1 signal has a protective effect on MI/RI, and importantly, hairy and enhancer of split 1 (Hes1) and YRPW motif 1 (Hey1) are the target genes of Notch1 [35]. Notch1/Hes1 signal has been demonstrated to modulate Tensin homolog (PTEN)/Akt pathway against MI/RI [36]. Furthermore, Notch1/Hes1 pathway can sustain NF-κB activation to regulate inflammation and protect cardiomyocytes from injury [37]. Another one downstream protein of Notch1 is NOX4 (NADPH Oxidase 4). Notch-NOX4-ROS signaling pathway can induce cell death and modulate huma retinal endothelial cell proliferation, migration and adhesion [38,39]. Previous study have revealed that NOX4 plays a dominant role in cardiomyocytes, and NOX4 knockout mice can reduce ROS production and attenuate the infarct size after ischemia-reperfusion [40]. In addition, NOX4 can regulate Nrf2 (nuclear factor erythroid-2 related factor 2) and glutathione (GSH) redox in cardiomyocytes [41]. Nrf2 is the main transcription factor for the activation of GCLC [42]. Some drugs or compounds to treat MI/RI are achieved through the Notch signaling pathway, such as relaxin, curcumin and remifentanil preconditioning [43–45]. Therefore, Notch1 signal is an effective pathway to treat MI/RI by inhibiting oxidative stress and inflammation.

Reducing MI/RI is an effective mean to improve the survival rate of myocardial infarction patients. In the present work, a novel MI/RI-associated factor circRNA named circMIRIAF was discovered, which sponged miR-544 to enhance WDR12 expression, thereby aggravating MI/RI by regulating the Notch1 signaling pahtway, which should be considered as a novel therapeutic strategy to treat MI/RI.

2. Materials and methods

2.1. AC16 cells culture and transfection

Human cardiomyocyte AC16 cells was purchased from Shanghai Hengya Biotechnology Co., Ltd. It was cultured in DMEM cell culture medium containing 10% FBS at 37°C and 5% CO_2. In the study, circMIRIAF (hsa_circ_0006174) overexpression vector plasmid (pCD5-ciR), circMIRIAF siRNA, miR-544 inhibitor and WDR12 overexpression vector plasmid were constructed and transfected into AC16 cells.

2.2. Animals, treatment and transfection

C57BL/6 male mice (weighing 18–22 g) were purchased from Liaoning Changsheng Biotechnology Co., Ltd. (production license: SCXK (Liao) 2020-0001), and the experimental unit use license (SCXK (Liao) 2018-0007). The animal experiment was performed accordance with China's legislation on the Use and Care of laboratory animals, and it was approved by the Animal Care and Use Committee of Dalian Medical University. All the animals were fed in an environment with a room temperature of 25 ± 2°C and a relative humidity of 60 ± 10%.

circMIRIAF (mmu_circ_0011688) shRNA and miR-544 antagomir were constructed and transfected into mice by tail vein injection respectively, injected every other day, and repeated 3 times. On the basis, MI/RI model was established by ligating the left anterior descending coronary artery for 30 min and reperfusion for 24 h [46]. Electrocardiogram (ECG) and echocardiography were monitored, and the levels of cardiac troponin I (cTn-I) and creatine kinase isoenzyme-MB (CK-MB) in myocardial tissue were detected. Triphenyltetrazolium chloride (TTC) and Evans blue staining, hematoxylin-eosin staining (H&E) staining and Masson staining of myocardial tissue were performed. The levels of circMIRIAF, miR-544, WDR12, inflammatory factors, superoxide dismutase (SOD) and Notch1 signal related proteins were detected by RT-PCR and Western blot assays.

2.3. Mouse primary cardiomyocyte isolation and culture

Mouse primary cardiomyocyte isolation kit (Applied cell, Shanghai, China) was used to extract cardiomyocytes from neonatal C57BL/6 mice. The heart of mouse was removed, and atrium was cut off. The tissue was cut into tissue blocks with a size of 1 mm^3. Then, an appropriate amount of Mouse Cell Dissociation Solution I was used to digest the tissue mass for overnight at 4°C. The second day, Mouse Cell Dissociation Solution II was added and shocked for 7 min at 37°C, then the supernatant was collected. This process was repeated multiple times until the tissue is completely digested. Next, the collected supernatant was centrifuged at 1200 rpm for 5 min, and re-suspended by Mouse Cardiomyocytes Culture Medium, and filtered through a 100 μm filter screen. Next, the cells are directly inoculated into the culture dish and incubated in an incubator with 5% CO_2 for 60–75 min at 37°C. After that, the supernatant was remove to new culture dish and incubated in an incubator with 5% CO_2 for 60–75 min at 37°C. Finally, the supernatant was centrifuged at 530 rpm for 5 min, and the cell precipitation was re-suspended by the culture. After 2–3 days of culture, the cells were used for the follow-up test [47].

2.4. MTT assay

AC16 cells were inoculated into 96 well plates. When the cell density was increased to 80%, the cells in control group was replaced with serum-free medium and cultured in 5% CO_2 at 37°C. The medium in H/RI (hypoxia-reoxygenation injury) group was replaced with PBS solution. After hypoxia for 24 h under certain conditions (1% O_2, 5% CO_2 and 94% N_2), PBS solution was replaced with serum-free DMEM culture medium, and the cells were normal cultured in incubator (37°C, 5% CO_2) for 1 h. MTT assay was used to detect cell viability.

2.5. LDH release detection

AC16 cells were inoculated into 96 well plate. As the cell density was increased to 80%, the DMEM cell culture medium was sucked and washed with PBS solution once. After replacing 1% FBS DMEM culture medium, the cells were divided into control group (Experimental group 1), non-H/RI treatment control group (Culture medium background), and non-H/RI treatment follow-up lysis group (Maximum LDH release). H/RI group (Experimental group 2) was set on another culture plate.

After treatment according to the experimental requirements, LDH releasing agent was added and the cells were incubated for a certain time. The supernatant was transferred into 96 well enzyme label plate, and the absorbance was measured at 490 nm. The level of LDH release was calculated according to the followed formula.

$$LDH\ release(\%) = \frac{Experimental - Culture\ medium\ background}{Maximum\ LDH\ release - Culture\ medium\ background} \times 100\%$$

2.6. Measurement of intracellular ROS level

AC16 cells were inoculated into 6-well plates, control group with serum-free medium was cultured under 37°C, 5% CO_2, H/RI group with PBS solution was placed in an incubator (1% O_2, 5% CO_2, 94% N_2) for 24 h. After that, it was replaced with serum-free culture medium for 1 h re-oxygenation. After adding DCFH-DA diluent (1: 1000) and incubating for 20 min, the cells were washed for 3 times by PBS, which were then observed and photographed by the inverted fluorescence microscope (Olympus, Tokyo, Japan).

2.7. circRNA microarray screening analysis

AC16 cells in control group and H/RI group were collected for Arraystar Human circRNA Array V2 analysis, and mouse primary cardiomyocyte in control group and H/RI group were collected for mouse circRNA Array analysis. Firstly, the total RNA was extracted. Next, RNA samples were prepared and microarray were hybridized according to arraystar scheme. The circRNAs were hybridized to Arraystar Human circRNA Array V2 (8 × 15K), and the array was scanned with Agilent Scanner G2505C.

Agilent feature extraction software (version 11.0.1.1) and R software limma package was applied for analysis. Finally, the differentially expressed circRNAs were screened by volcano plot filtering, and then identified by folding change filtering. The distinguishable circRNAs patterns were displayed by hierarchical clustering.

2.8. RNA-seq analysis

AC16 cells in control, H/RI, circMIRIAF siRNA and miR-544 inhibitor treatment groups were collected to extract total RNA samples, which were subjected to agarose electrophoresis. After determination, the sequencing library was constructed. Total of 1–2 μg RNA was pre-processed (rRNA removal), and the library was constructed by Illumina hiseq 4000. FastQC software was used to evaluate the sequencing quality of reads after splicing (cut the 3′ and 5′ connectors), and the reference genome was compared through Hisat2 software. After screening the differentially expressed genes, principal component analysis (PCA), clustering of Pearson correlation coefficient of gene expression levels among samples, GO and pathway analysis were carried out.

2.9. ceRNA analysis

The potential binding sites of target circRNA (circMIRIAF), miRNA and mRNA were predicted by circnet database (http://bigd.big.ac.cn/databasecommons/database/id/1751), and the network of circRNA-miRNA-mRNA was constructed.

2.10. Fluorescence in situ hybridization probe detection (FISH)

Fluorescent probes were designed according to circMIRIAF and miR-544 sequences. AC16 cells inoculated into 48-well plate were cultured overnight and then washed by PBS solution. 4% paraformaldehyde was added to fix the plate for 15 min. The next steps were carried out according to the instruction of FISH kit (Shanghai Genepharma Co., Ltd), and the cell localization was detected by laser scanning confocal image system (TCS SP5II, Leica, Germany).

2.11. Dual-luciferase reporter gene experiment

According to the 3′UTR sequence of circMIRIAF and WDR12, wild-type (wt) and mutant (mut) sequences of circMIRIAF and WDR12 were synthesized, and the plasmid was constructed by pmiR-RB-REPORTTM. In AC16 cells, wt and mut plasmids were transfected with miR-544 mimic, respectively. In order to verify the relationship between circMIRIAF and miR-544, the experiment were performed on the groups of circMIRIAF-wt + NC, circMIRIAF-wt + miR-544 mimic, circMIRIAF-mut + NC and circMIRIAF-mut + miR-544 mimic. In order to confirm the relationship between miR-544 and WDR12, the experiment were performed on the groups of WDR12-wt + NC, WDR12-wt + miR-544 mimic, WDR12-mut + NC and WDR12-mut + miR-544 mimic. The operation process was as follows: AC16 cells were inoculated into 24-well plates. When the cell density reached to 50–60%, lipofectamine2000 was used for the transfection. After 24 h pretreatment, fluorescence assays were carried out according to kit (Shanghai Genepharma Co., Ltd). The amplification primers constructed by dual-luciferase vector are shown in Supplementary Table S1.

2.12. RNA-binding protein immunoprecipitation (RIP)

Magna RIP RNA-Binding Protein Immunoprecipitation Kit (Millipore, Billerica, MA, USA) was used for RIP. AC16 cells was prepared for the experiment. Finally, Ago2 protein was detected, and the enrichment levels of circMIRIAF, miR-544 and WDR12 were detected, too.

2.13. circRNA pull down

circRNA pull down experiment was performed as previously mentioned [48]. The process was provided in Supplementary material.

2.14. miRNA binding profile of target circRNA

The RNA antisense purification experiment was carried out for miRNA binding profile of target circRNA. The circMIRIAF probe was designed using connector sequence, which was synthesized by BersinBio (Guangzhou, China). Then, the BersinBioTM RNA antisense purification kit (BersinBio, Guangzhou, China) was used to purify RNA sample, which was evaluated by NanoDrop ND-1000. Then, mouse miRNA oligonucleotide microarray was used (Supplementary material).

2.15. Assessment of biochemical parameters

The levels of cTn-I and CK-MB in serum were measured by the commercial kits (Nanjing Jiancheng Bioengineering institute, Nanjing, China). Myocardial tissue homogenate was prepared according to the instruction of the kit to detect SOD level.

2.16. ECG detection in mice

After anesthesia with isoflurane, the mice were fixed on the mouse fixation plate. According to the requirements of ECG instrument (IX-BIO4, iWorx, USA), the ends of five wires were insert under the skin of mice's limbs. The ECG of mice were recorded by the workstation.

2.17. Echocardiography of mice

Echocardiography was carried out on mice using VINNO 6VET/6LAB digital Protable Ultrasound Scanner (VINNO, China). The M-mode was performed through the middle of the left ventricle and the maximum diameters was seen by adjusting the ultrasound beam carefully.

2.18. Pathological examination of mouse myocardium

The myocardial tissues of mice were collected and fixed with 10% formalin, embedded with paraffin, made into paraffin slices, stained with H&E and Masson, photographed with optical microscope (Eclipse C1, Nikon, Japan).

After myocardial ischemia-reperfusion 24 h, the mouse heart was retrogradely injected with Evans blue from the aorta. Then, the heart removed form mouse, and it was frozen and sectioned into slices. Next, the slices were soaked in 1% TTC solution for 10 min at 37°C. Further, those slices were immersed in 4% paraformaldehyde over night. The non-ischemic area of slices was blue, and the infarct area was white, and the non-infarct area at risk was red. Finally, Image acquisition was carried out by panoramic slice scanner. And Image-Pro Plus 6.0 analysis software was used measure the pixel area of each tissue, and calculate the proportion of myocardial infarction.

The methods of Quantitative real-time PCR, Western blot and Statistical analysis are provided in Supplementary material.

3. Results

3.1. Prediction of circRNA-miRNA-mRNA axis

3.1.1. Establishment of AC16 cell H/RI model and mouse MI/RI model

The viability of AC16 cells was significantly decreased after hypoxia for 24 h and re-oxygenation for 1 h ($P < 0.05$), which was decreased to 48.02 ± 7.07% in control group (Fig. 1A). LDH release was increased after 24 h of hypoxia and 1 h of re -oxygenation (Fig. 1B). The changes in cell morphology indicated that 24 h hypoxia and 1 h re-oxygenation injury caused cell apoptosis (Fig. 1C). In addition, ROS level and the mRNA levels of *IL-1β*, *IL-6*, *TNF-α*, *ICAM-1* in H/RI group were increased (Fig. 1D and E). Thus, H/RI model in AC16 cells was established by 24 h hypoxia and 1 h re-oxygenation.

ST segment of ECG in MI/RI group was elevated (Supplementary Fig. S1A), and serum CK-MB and cTn-I levels were increased compared with sham group (Supplementary Fig. S1B). Further, in MI/RI group, the white non-viable infarct, the red injured tissue, the blue non injured tissue, the decreased thickness left ventricular wall, and the infarct size (% risk area) at 36.65 ± 5.43% were found (Supplementary Fig. S1C–D). In addition, myocardial fibers, transverse striations disappeared, sarcoplasma dissolved, irregular granules, masses and contractile bands were formed in MI/RI group (Supplementary Fig. S1E). SOD levels were decreased ($P < 0.01$), and the mRNA levels of *IL-1β*, *IL-6*, *TNF-α* and *ICAM-1* were increased in MI/RI group compared with sham group ($P < 0.01$) (Supplementary Fig. S1F–G).

3.1.2. Expression pattern of circRNAs in H/RI AC16 cells

Before Arraystar Human CircRNA Array V2 analysis, the results of RNA integrity and gDNA contamination test of control and model (H/RI) groups of AC16 cells showed that the quality of experimental sample met the requirements (Supplementary Fig. S2A). The heatmap of hierarchical clustering of all expressed circRNAs are shown in Supplementary Fig. S2B. Total of 13406 circRNAs were identified in AC16 cells, and the heatmap of hierarchical clustering of differentially expressed circRNAs of control and model (H/RI) groups is shown in Fig. 1F (Fold Change cut-off: 2.0, *P*-value cut-off: 0.05), in which 92 differentially expressed circRNAs were up-regulated, and 9 differentially expressed circRNAs were down-regulated (Supplementary Table S2).

3.1.3. circMIRIAF was highly expressed in H/RI AC16 cells

Among the differentially expressed circRNAs, the candidate circRNAs were consistent with the following conditions (raw intensity is higher than 200; the length of base sequence is in the range of 100–3000; homology with mouse circRNAs is greater than 70%). In the study, 8 candidate circRNAs with differentially expression were screened out (Table 1), which were marked in the volcanic map (Fig. 1G). The raw intensity and the validation results by RT-PCR assay are shown in Fig. 1H and I. hsa_ circRNA_103114, hsa_circRNA_006752, hsa_circRNA_092556, hsa_circRNA_104852 and hsa_circRNA_104854 were significantly up-regulated in H/RI group compared with control group. Among them, hsa_circRNA_104852 was transcribed by RAD23B, which was stably expressed in myocardial cells. RAD23B can transcribe a variety of circRNAs with different physiological roles [49,50]. hsa_circRNA_104852 plays the critical role in the occurrence and development of cancer, which can accelerate colorectal cancer progression through regulating miR-138-5p/MACC1 axis [51], and exosomal transfer of it contributes to the chemoresistance of doxorubicin in colorectal cancer by depending on miR-1205/CCND2 axis [52]. hsa_circRNA_104852 can also promote colorectal cancer progression by sponging microRNA-142-3p and regulating X-linked inhibitor of apoptosis expression [53]. The present study found that hsa_circRNA_104852 was also highly expressed in myocardial cells during H/RI, which should play an important role in MI/RI and be considered as one biomarker or drug therapy target for the disease. hsa_circRNA_104852 has the highest homology of 98% with mmu_circ_0011688. hsa_circRNA_104852 encoded by RAD23B is located in chr9: 110064315-110068928, and mmu_circ_0011688 encoded by RAD23B is located in chr4: 55379648-55380996 (Fig. 1J). hsa_circRNA_104852 and mmu_circ_0011688 are encoded by RAD23B, and mmu_circ_0011688 is used for verification on animal level. The results of fluorescence probe in situ hybridization experiments indicated that hsa_circRNA_104852 exists in AC16 cells, and mmu_circ_ 0011688 exists in mouse heart tissue (Fig. 1K). In the study, hsa_circRNA_104852 and mmu_circ_0011688 were named as circRNA MI/RI-associated factor (circMIRIAF). In addition, the levels of circMIRIAF in heart tissue of MI/RI mice and mouse primary cardiomyocytes with H/RI were increased (Fig. 1L). Eventually, circMIRIAF was selected as the target circRNA.

3.1.4. ceRNA analysis

The RNA-seq results of AC16 cells showed that 5117 differentially expressed genes were identified between control and model (H/RI) groups (log2FC cut-off: 0.585, *P*-value cut-off: 0.05), in which 3996 were up-regulated and 1121 were down-regulated. The correlation coefficient of the samples in RNA-seq assay, genes volcano_plot, and heatmap of the differential genes of model vs. control are shown in Supplementary Fig. S2C–E.

Based on the circMIRIAF and the differentially expressed genes with up-regulation, ceRNA assay was performed to predict related miRNAs and form a network (Fig. 2A). According to the prediction, 11 miRNAs had binding site with circMIRIAF, and 5 of them had binding site with up-regulated differential genes, including hsa-miR-708-5p/*ZNF891*, hsa-miR-28-5p/*ZNF891*, hsa-miR-20b-3p/*ECI2*, hsa-miR-766-5p/*THADA*, *BCKDHB*, and hsa-miR-544a/*WDR12*. The validation results of those miRNAs in AC16 cells showed in Fig. 2B. The expression level of hsa-miR-708-5p was up-regulated, and hsa-miR-766-5p level had no significant change in H/RI group. The levels of hsa-miR-28-5p, hsa-miR-20b-3p and hsa-miR-544a were down-regulated in H/RI group, which should be the targets of circMIRIAF sponge adsorption. Some reports have shown that miR-544a located at 14q32.31 can regulate inflammation in spinal cord injury, induce epithelial mesenchymal transition of gastric cancer, and stimulate endometrial cancer growth [54–56]. miR-544 can also attenuate diabetic renal injury via suppressing glomerulusclerosis and inflammation by targeting fatty acid synthase (FASN) [57], which may participate in controlling inflammation and apoptosis after cerebral ischemia-reperfusion, and providing possible diagnostic indicators and therapeutic targets [58]. Thus, miR-544 may attenuate MI/RI by regulating inflammatory response, which was selected for further investigation. In the study, hsa-miR-544a (5′-AUUCUGCAUUUUUAGCAAGCUC-3′) and mmu-miR-544-3p (5′-AUUCUGCAUUUUUAGCAAGUUC-3′) were named miR-544. In addition, the gene levels of *ZNF891*, *ECI2*, *THADA*, *BCKDHB* and *WDR12*

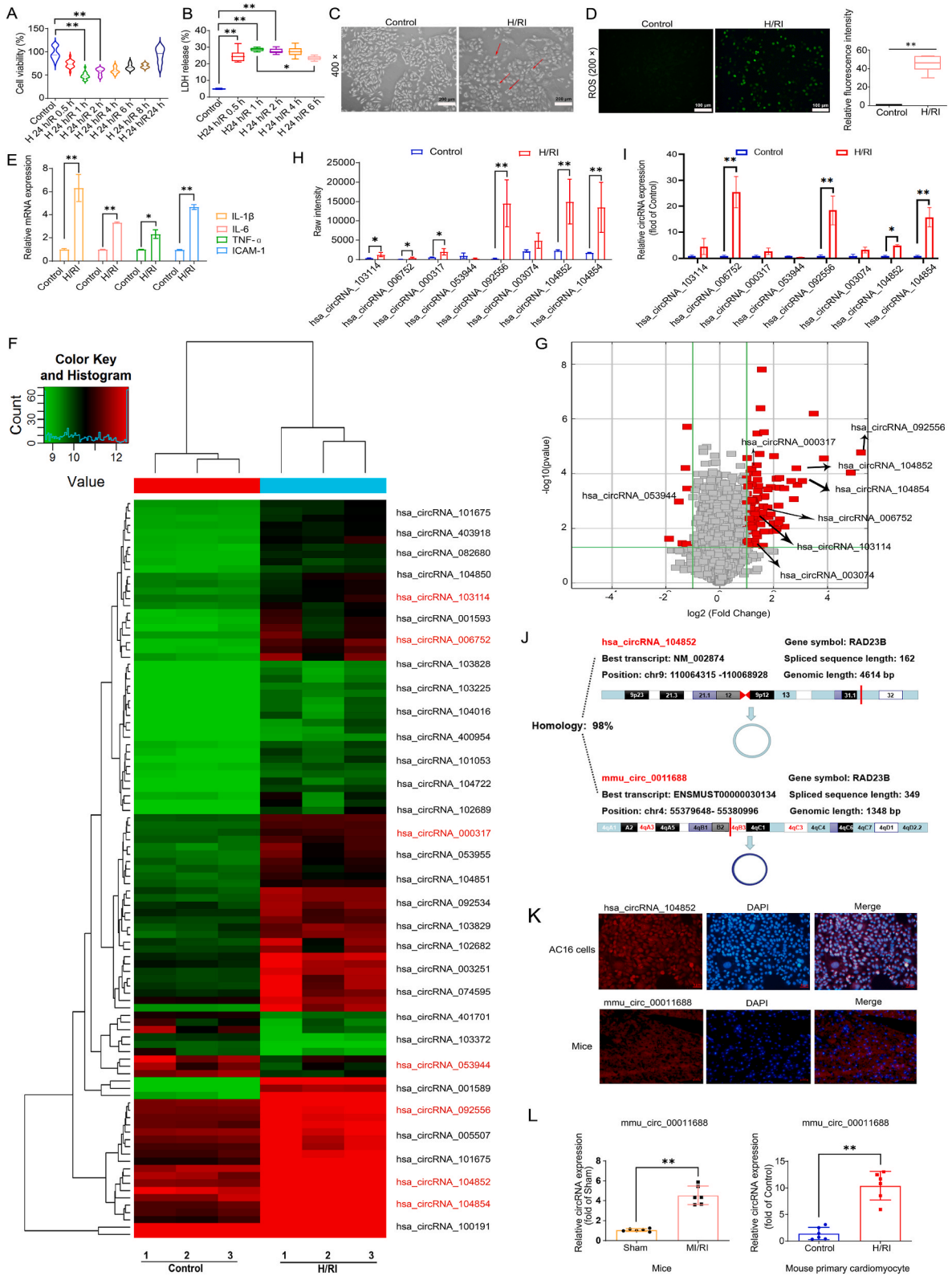

Fig. 1. Establishment of hypoxia-reoxygenation injury model in AC16 cells for targeted circRNAs selecting. (**A**) Cell viability of AC16 cells under different re-oxygenation times (n = 6). (**B**) LDH release of AC16 cells under different re-oxygenation times (n = 6). (**C**) Effects of H 24 h/R 1 h injury (H/RI) on cell morphology of AC16 cells (n = 3). (**D**) Effects of H/RI on ROS level in AC16 cells (n = 3). (**E**) Effects of H/RI on mRNA levels of *IL-1β*, *IL-6*, *TNF-α* and *ICAM-1* in AC16 cells (n = 6). (**F**) Heatmap of H/RI group compared with control group (n = 3). (**G**) The volcanic map of differentially expressed circRNAs and the candidate target circRNAs (n = 3). (**H**) Raw intensity of the candidate circRNAs in Arraystar Human CircRNA Array V2 analysis (n = 3). (**I**) RT-PCR validation results of the candidate circRNAs (n = 3). (**J**) Information of hsa_circ_0006174 (hsa_circRNA_104852) and mmu_circ_0011688. (**K**) The results of situ hybridization experiments of hsa_circ_104852 in AC16 cells and mmu_circ_ 0011688 in mouse heart tissue (n = 3). (**L**) The expression level of circMIRIAF in mouse heart tissue and mouse primary cardiomyocytes (n = 6). Data are shown as mean ± SD. $^{*}P < 0.05$, $^{**}P < 0.01$.

Table 1
Candidate circRNAs information.

Alias	circRNA	Fold Change	Chrom	GeneSymbol
hsa_circ_0006174	hsa_circRNA_104852	7.1639867	chr9	RAD23B
hsa_circ_0000317	hsa_circRNA_000317	2.576725	chr11	AHNAK
hsa_circ_0087862	hsa_circRNA_104854	8.3683495	chr9	RAD23B
hsa_circ_0001583	hsa_circRNA_092556	37.7872806	chr6	HIST1H1C
hsa_circ_0003074	hsa_circRNA_003074	2.4358923	chr10	DHTKD1
hsa_circ_0006752	hsa_circRNA_006752	2.0185908	chr22	NF2
hsa_circ_0003323	hsa_circRNA_103114	2.2856746	chr21	APP
hsa_circ_0053944	hsa_circRNA_053944	0.4212434	chr2	FAM98A

in H/RI group were up-regulated compared with control group (Fig. 2C). WDR12 with high expression in failing hearts can cause deterioration of cardiac function [59]. Therefore, circMIRIAF/miR-544/WDR12 axis was found as one possible target on regulating MI/RI.

3.2. Verification of circMIRIAF/miR-544/WDR12 axis

The FISH results in Fig. 2D indicated that circMIRIAF and miR-544 were co-located in cytoplasm of AC16 cells, and circMIRIAF should exert its effect through sponge adsorption of miR-544. Then, the dual-luciferase reporter gene assay was used to predict and identify the binding site of circMIRIAF and miR-544, as well as the binding site of WDR12 and miR-544. The result exhibited that miR-544 mimic inhibited the luciferase activity of circMIRIAF-wt. However, there was no significant difference between circMIRIAF-mut-NC group and circMIRIAF-mut + miR-544 group (Fig. 2E). Thus, miR-544 was a target of circMIRIAF. Further, miR-544 mimic inhibited the luciferase activity of WDR12-wt group, but there was no significantly difference between WDR12-mut-NC group and WDR12-mut + miR-544 group (Fig. 2E). These data confirmed that WDR12 was a target of miR-544.

The expression level of miR-544 in heart tissue of MI/RI mice was also decreased (Fig. 2F). Furthermore, circMIRIAF was silenced and overexpressed in AC16 cells, and the results showed circMIRIAF knockdown strikingly increased the expression of miR-544, and circMIRIAF overexpression strikingly decreased the expression of miR-544 (Fig. 2G). RIP results showed the relative enrichment of circMIRIAF, miR-544 and WDR12 levels in anti-Ago2 group were significantly increased compared with anti-IgG group (Fig. 2H), indicating that circMIRIAF, miR-544 and WDR12 were co-enriched. The data in Fig. 2I showed that the biotin probes of circMIRIAF had achieved a large amount of enrichment to precipitate Ago2 protein and pull down miR-544. The heatmap of all miRNAs enriched by circMIRIAF probes is shown in Supplementary Fig. S3. The top 20 miRNAs of circMIRIAF probes co-enriched is shown in Fig. 2J, and miR-544 was one of them. Thus, circMIRIAF competitively adsorbed miR-544 to reduce the inhibition of miR-544 on WDR12.

3.3. WDR12/Notch1 signaling pathway participates in MI/RI

GO pathway assay of the differentially expressed genes of H/RI AC16 cells group compared with control group showed that Notch_signaling_pathway, negative_regulation_of_Notch_signaling_pathway, positive_regulation_of_Notch_signaling_pathway and regulation_of_Notch_signaling_pathway, Notch_signaling_involved_in _heart development were participate in MI/RI process, and Notch signal pathway of KEGG analysis is shown in Supplementary Fig. S4. The expression levels of WDR12 and its downstream related proteins in AC16 cells and mice are shown in Fig. 2K. The expression levels of WDR12, NOX4, p-P65, IL-1β, IL-6, TNF-α and ICAM-1 in model groups were up-regulated, and the expression levels of Notch1, Activated Notch1, Nrf2, GCLC, Hes1, Hey1 were significantly down-regulated. All the results indicated that circMIRIAF/miR-544/WDR12 regulated oxidative stress and inflammation of MI/RI via Notch1 signal pathway *in vitro* and *in vivo*.

3.4. miR-544 inhibition aggravates H/RI of AC16 cells

The effects of miR-544 inhibitor on cell viability and LDH release in H/RI of AC16 cells are shown in Fig. 3A. Cell viability was decreased in inhibitor-NC + H/RI group compared with inhibitor-NC group. After miR-544 treatment, the cell viability of AC16 cells was further decreased. Meanwhile, LDH release was increased in inhibitor–NC + H/RI group compared with inhibitor-NC group, which was further increased after miR-544 inhibitor treatment. Thus, miR-544 inhibition decreased cell viability and increased LDH release in AC16 cells.

The expression levels of circMIRIAF and miR-544 are shown in Fig. 3B. After H/RI, circMIRIAF level in AC16 cells was up-regulated. However, there was no significant difference before and after miR-544 inhibitor treatment. miR-544 level in AC16 cells was down-regulated after H/RI, which was further decreased after miR-544 inhibitor treatment ($P < 0.01$). Thus, miR-544 inhibition decreased miR-544 level and increased ROS levels in AC16 cells (Fig. 3C). In addition, the mRNA levels of *IL-1β*, *IL-6*, *TNF-α* and *ICAM-1* in Fig. 3D proved that miR-544 inhibitor exacerbated inflammatory response during H/RI in AC16 cells.

The effects of miR-544 inhibitor on the protein expression levels of WDR12 and Notch1 signal in AC16 cells are shown in Fig. 3E. The protein level of WDR12 was up-regulated after H/RI, and Notch1, Activated Nothch1 levels were down-regulated. The protein levels of NOX4, p-P65, IL-1β, IL-6, TNF-α and ICAM-1 were up-regulated, and Nrf2, GCLC, Hes1 and Hey1 levels were down-regulated after H/RI. After miR-544 inhibitor treatment, the protein level of WDR12 was further increased, and Notch1, Activated Nothch1 levels were further decreased. The levels of downstream proteins in Notch1 pathway were also changed. Based on the above experiments, the results showed that miR-544 inhibitor was positively correlated with WDR12 (Correlation coefficient: 0.46), while miR-544 was negatively correlated with WDR12 (Correlation coefficient: −0.78) (Fig. 3F). To further elucidate the effect of the miR-544 on H/RI, RNA-seq analysis was performed on AC16 cells transfected with miR-544 inhibitor. The results of differentially expressed gene showed miR-544 inhibitor also induced oxidative stress and inflammatory response in AC16 cells, and exacerbated the H/RI of AC16 cells (Supplementary Fig. S5–S6). Thus, miR-544 negatively regulated WDR12 expression to aggravate oxidative stress and inflammatory though Notch1 signal.

3.5. miR-544 inhibition aggravates MI/RI of mice

The miR-544 antagomir decreased the cardiac function of MI/RI mice. The ST segment was elevated after MI/RI, which were further elevated in miR-544 antagomir treated mice (Fig. 4A). The myocardial infarct size was increased ($P < 0.01$), and the left ventricular wall thickness was decreased ($P < 0.05$) in miR-544 antagomir treated mice after MI/RI (Fig. 4B). The echocardiography of mice heart is shown in Fig. 4C, the levels of %EF and %FS were decreased, and the LVIDs and LVIDd were decreased ($P < 0.05$) in miR-544 antagomir treated mice after MI/RI. Further, the heart rate of mice in the antagomir-NC + MI/RI group was 417 ± 23 bpm, it was increase to 444 ± 36 bpm in miR-544 antagomir + MI/RI group.

In addition, the arrangement of myocardial fibers in antagomir-NC

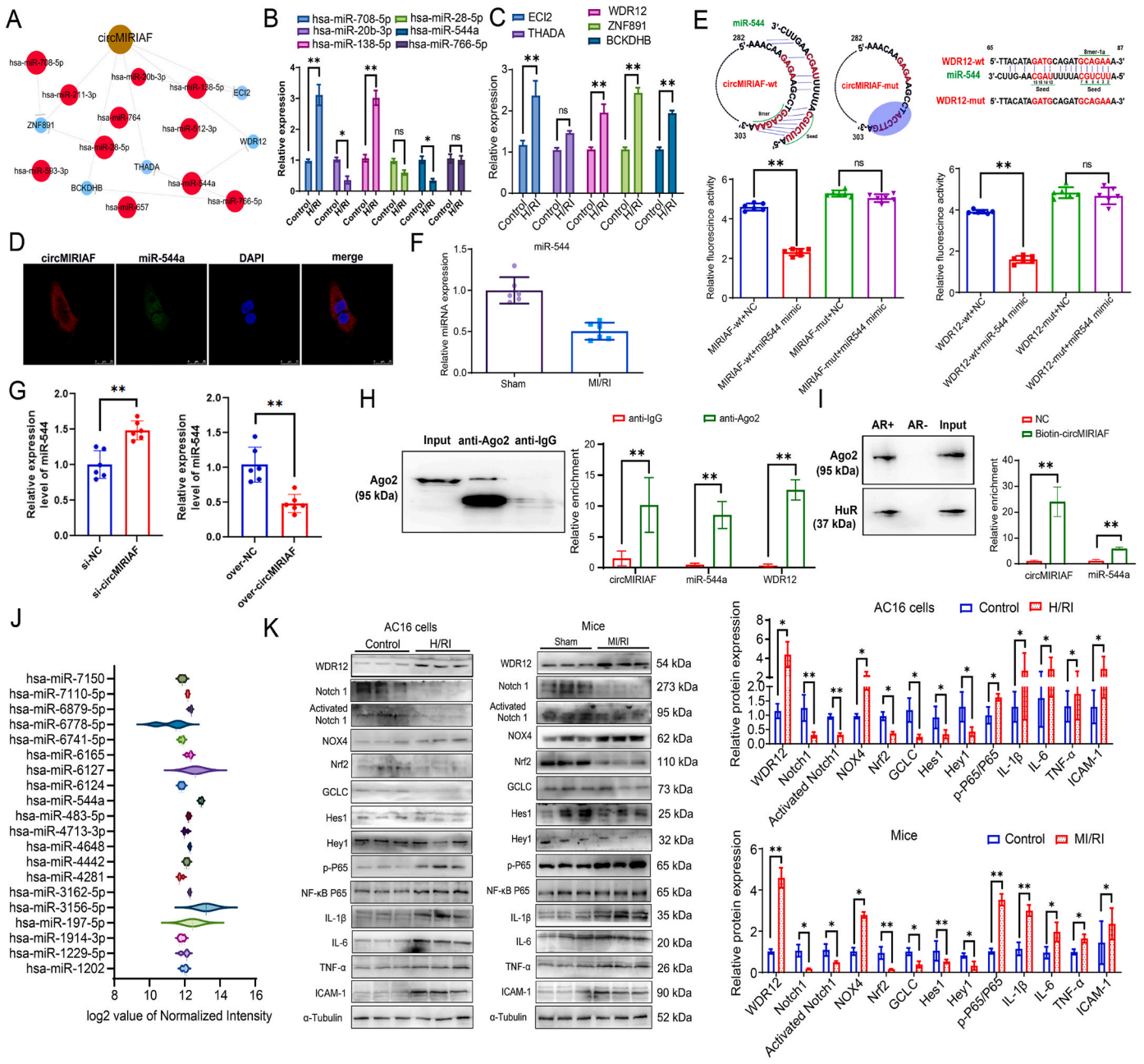

Fig. 2. Analysis and validation results of ceRNA relationship. (**A**) Network of circMIRIAF ceRNA analysis. (**B**) The expression levels of hsa-miR-708-5p, hsa-miR-28-5p, hsa-miR-138-5p, hsa-miR-20b-3p, hsa-miR-766-5p and hsa-miR-544a in H/RI AC16 cells (n = 6). (**C**) The mRNA levels of *ZNF891*, *ECI2*, *THADA*, *BCKDHB* and *WDR12* in H/RI AC16 cells (n = 6). (**D**) Localization of circMIRIAF and miR-544 in AC16 cells by FISH (n = 3). (**E**) Prediction of binding sites between circMIRIAF and miR-544, WDR12 and miR-544, and mutant amplification primers, and the result of double luciferase gene report experiments (n = 3). (**F**) The expression level of miR-544 in mouse heart tissue (n = 6). (**G**) The expression level of miR-544 in AC16 cells transfected with circMIRIAF siRNA and circMIRIAF overexpression plasmid (n = 6). (**H**) RIP was utilized to examine the combination between circMIRIAF and miR-544, miR-544 and WDR12 (n = 3). (**I**) circRNA pull down was utilized to examine the combination between circMIRIAF and miR-544 (n = 3). Biotinylated circMIRIAF was incubated with total AC16 cell extracts, targeted with streptavidin beads, and washed. AR bind to HuR was served as a positive control (AR+). (**J**) The top 20 miRNAs bind to circMIRIAF (n = 3). (**K**) The expression levels of WDR12 and its downstream proteins in H/RI AC16 cells and MI/RI mice (n = 3). Data are shown as mean ± SD. $^{*}P < 0.05$, $^{**}P < 0.01$, *ns* is no significant difference.

group was dense. But, the cells of left ventricular outer wall were incomplete and broken in antagomir-NC + MI/RI group and miR-544 antagomir + MI/RI group, and miR-544 antagomir increased the infiltration of inflammatory cells in myocardial tissue (Fig. 4D and E). Further, miR-544 antagomir increased serum CK-MB and cTn-I levels in MI/RI mice (Fig. 4F). The serum levels of CK-MB and cTn-I in miR-544 antagomir + MI/RI group were increased compared with antagomir-NC + MI/RI group. The levels of circMIRIAF and miR-544 in mice are shown in Fig. 4G and H. For circMIRIAF, its level was increased in mice after MI/RI, but there was no significant change before or after miR-544 antagomir treatment. For miR-544, its level was decreased in mice after MI/RI, which was further down-regulated after miR-544 antagomir treatment. As shown in Fig. 4I, the mRNA levels of *IL-1β*, *IL-6*, *TNF-α* and *ICAM-1* were increased in miR-544 antagomir group compared with antagomir-NC group, which were increased in miR-544 antagomir + MI/RI group compared with miR-544 antagomir group. In addition, SOD level in miR-544 antagomir group was decreased compared with antagomir-NC group, which was decreased in miR-544 antagomir + MI/

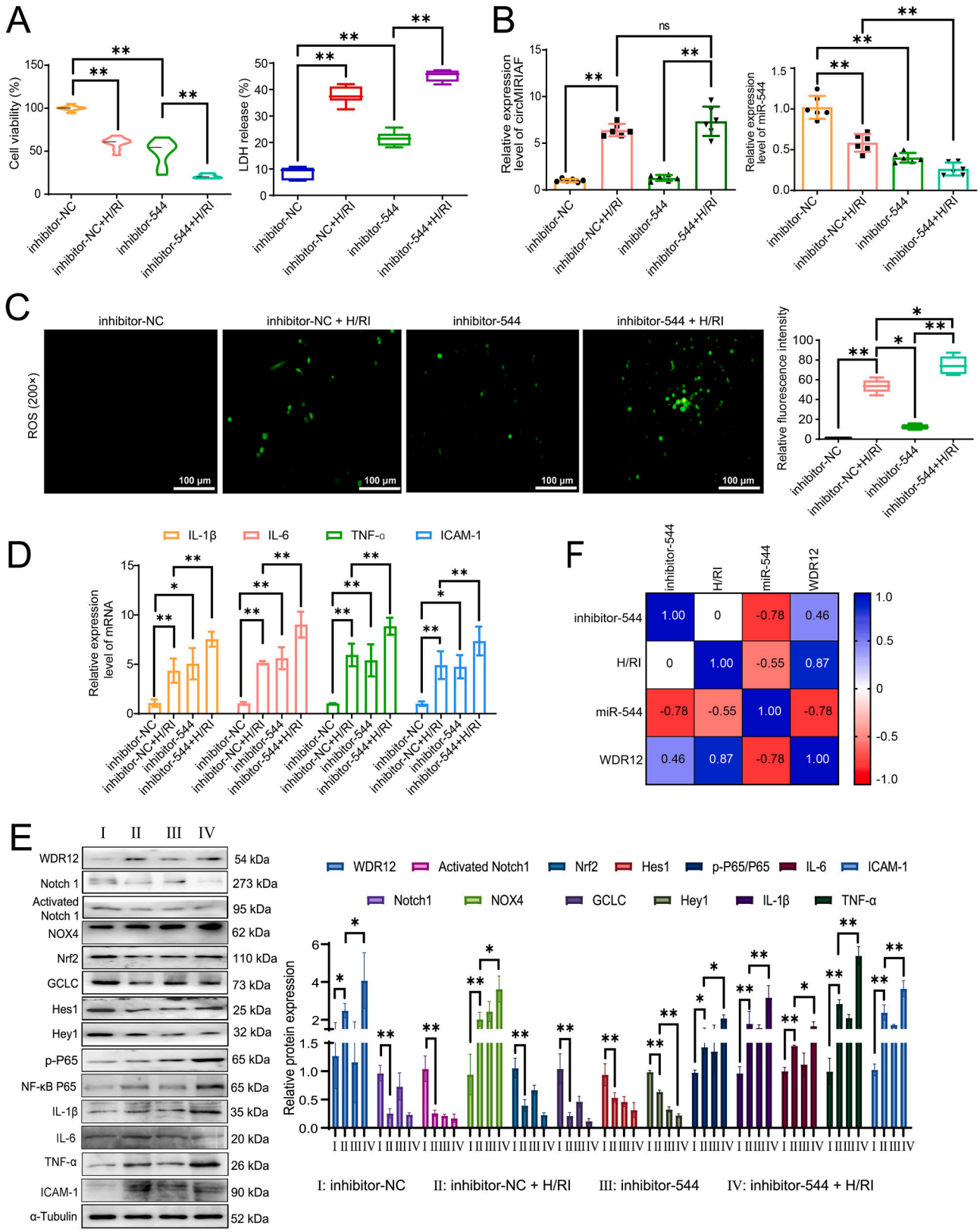

Fig. 3. miR-544 inhibitor aggravates H/RI of AC16 cells. (**A**) Cell viability and LDH release of H/RI AC16 cells transfected with miR-544 inhibitor (n = 6). (**B**) The expression levels of circMIRIAF and miR-544 of H/RI AC16 cells transfected with miR-544 inhibitor (n = 6). (**C**) The ROS level of H/RI AC16 cells transfected with miR-544 inhibitor (n = 3). (D) The expression levels of *IL-1β*, *IL-6*, *TNF-α* and *ICAM-1* of H/RI AC16 cells transfected with miR-544 inhibitor (n = 6). (E) The levels of WDR12, Notch1, Activated Notch1 and downstream proteins in H/RI AC16 cells transfected with miR-544 inhibitor (n = 3). (F) Correlation analysis of miRNA-544 inhibitor, H/RI with miR-544 and WDR12 expression. Data are shown as mean ± SD. $^{*}P < 0.05$, $^{**}P < 0.01$, *ns* is no significant difference.

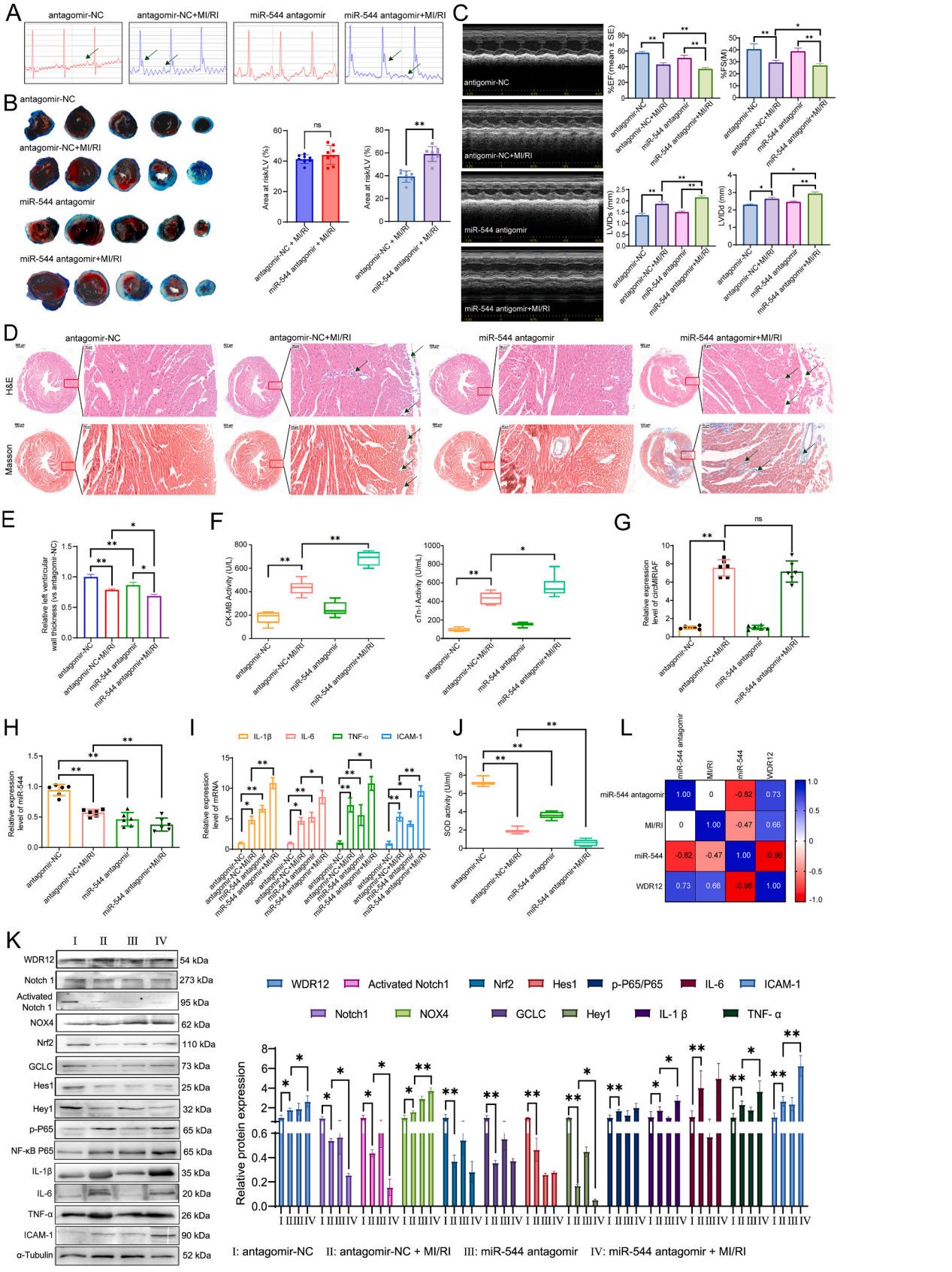

(caption on next page)

Fig. 4. miR-544 antagomir aggravates MI/RI in mice. (**A**) ECG of mice transfected with miR-544 antagomir (n = 3). (**B**) Representative images of TTC/Evans blue staining of the hearts of mice transfected with miR-544 antagomir. The ratios of area at risk (AAR) to left ventricular area (LV) and infarct size normalized to AAR are shown (n = 8). (**C**) Echocardiography of hearts of mice transfected with miR-544 antagomir (n = 5). (**D**) H&E and Masson staining of myocardial tissue of mice transfected with miR-544 antagomir, scale bars = 500 μm and 50 μm, n = 3. (**E**) The relative left ventircular wall thickness of myocardial tissue of mice transfected with miR-544 antagomir (n = 3). (**F**) The serum CK-MB and cTn-I levels of MI/RI mice transfected with miR-544 antagomir (n = 6). (**G**) The expression level of circMIRIAF of myocardial tissue of mice transfected with miR-544 antagomir (n = 6). (**H**) The expression level of miR-544 of myocardial tissue of mice transfected with miR-544 antagomir (n = 6). (**I**) The expression levels of *IL-1β*, *IL-6*, *TNF-α* and *ICAM-1* of myocardial tissue of mice transfected with miR-544 antagomir (n = 6). (**J**) The SOD level of myocardial tissue of mice transfected with miR-544 antagomir (n = 6). (**K**) The expression levels of WDR12, Notch1, Activated Notch1 and downstream proteins of myocardial tissue of mice transfected with miR-544 antagomir (n = 3). (**L**) Correlation analysis of miR-544 antagomir, MI/RI with miR-544 and WDR12 expression. Data are shown as mean ± SD. $^{*}P < 0.05$, $^{**}P < 0.01$, *ns* is no significant difference.

RI group compared with miR-544 antagomir group (Fig. 4J). Furthermore, miR-544 inhibition increased the protein level of WDR12 and decreased the expression levels of Notch1 and Activated Notch1 (Fig. 4K). Based on the above tests, the result showed that miR-544 antagomir was positively correlated with WDR12 (Correlation coefficient: 0.73), while miR-544 was negatively correlated with WDR12 (Correlation coefficient: −0.96) (Fig. 4L). Therefore, miR-544 negatively regulated WDR12 expression to aggravate oxidative stress and inflammation in MI/RI mice though Notch1 signal.

3.6. *circMIRIAF siRNA attenuates H/RI of AC16 cells, and circMIRIAF overexpression aggravates H/RI of AC16 cells*

The effects of circMIRIAF on AC16 cell viability and LDH release are shown in Fig. 5A–B**.** Cell viability of AC16 cells was decreased after H/RI, which was significantly increased by circMIRIAF siRNA, and reduced by circMIRIAF overexpression plasmid. Cell viability was increased in si-circMIRIAF + H/RI group compared with si-NC + H/RI group, which was decreased in over-circMIRIAF + H/RI group compared with over-NC + H/RI group.

The level of circMIRIAF in AC16 cells is shown in Fig. 5C. circMIRIAF siRNA achieved inhibition effect on circMIRIAF expression, and circMIRIAF overexpression plasmid achieved overexpression of circMIRIAF. The level of circMIRIAF was increased after H/RI, which was decreased in si-circMIRIAF + H/RI group, and increased in over-circMIRIAF + H/RI group. The data in Fig. 5D showed that the level of miR-544 was decreased after H/RI in AC16 cells, which was increased in si-circMIRIAF + H/RI group, and decreased in over-circMIRIAF + H/RI group compared with over- NC + H/RI group. The data in Fig. 5E showed that the expression level of circMIRIAF and the mRNA levels of inflammatory factors were positively correlated. circMIRIAF increased ROS level in AC16 cells (Fig. 5F), which was decreased in si-circMIRIAF + H/RI group compared with si-NC + H/RI group. The effects of circMIRIAF siRNA and circMIRIAF overexpression plasmid on protein levels in WDR12/Notch1 signal pathway are shown in Fig. 5G. After H/RI, the expression level of WDR12 was increased, and the levels of Notch1 and Activated Notch1 were decreased. The levels of NOX4, NF-κB, IL-1β, IL-6, TNF-α and ICAM-1 were up-regulated, and the levels of Nrf2, GCLC, Hes1 and Hey1 were down-regulated. However, the levels of the proteins were reversed by cricMIRIAF siRNA in si-circMIRIAF + H/RI groups, which were further increased or decreased in over-circMIRIAF + H/RI group. Based on the above experiments, the result showed that circMIRIAF was negatively correlated with miR-544 (Correlation coefficient: −0.82), while circMIRIAF was positively correlated with WDR12 (Correlation coefficient: 0.88) (Fig. 5H). To further elucidate the effect of the circMIRIAF on H/RI, RNA-seq analysis also was performed on AC16 cells transfected with circMIRIAF siRNA. The results showed that circMIRIAF siRNA alleviated oxidative stress and inflammation in AC16 cells during hypoxia and reoxygenation (Supplementary Figs. S7 and S8). Thus, circMIRIAF regulated WDR12/Notch1 signal pathway by sponge adsorption of miR-544 to exacerbate H/RI in AC16 cells.

3.7. *circMIRIAF shRNA attenuates MI/RI of mice*

As shown in Fig. 6A, the results of ECG indicated that circMIRIAF shRNA significantly improved mice cardiac function and pathological damage induced by MI/RI. The ECG of mice in sh-NC group and sh-circMIRIAF group was in normal state, and ST segment was elevated in sh-NC + MI/RI group, while ST segment was depressed after circMIRIAF shRNA pre-treatment. The myocardial infarct size was increased ($P < 0.01$), and the left ventricular wall thickness was significantly decreased in sh-circMIRIAF + MI/RI group compared with sh-NC + MI/RI group (Fig. 6B). The echocardiography of mice heart is shown in Fig. 6C, the levels of %EF and %FS were increased, and the LVIDs and LVIDd were decreased in circMIRIAF siRNA treated mice after MI/RI ($P < 0.05$). In addition, the heart rate of mice in the sh-NC + MI/RI group was 414 ± 34 bpm, it was decrease to 404 ± 22 bpm in sh-circMIRIAF + MI/RI group.

Histopathological observation found that circMIRIAF shRNA had a protective effect on mice MI/RI. As shown in Fig. 6D and E, myocardial fibers arranged compactly and cell morphology was normal in sh-NC and sh-circMIRIAF groups. While, the left ventricular outer wall cells appeared incomplete state, and the arrangement of myocardium was disordered, myocardial necrosis, dissolution and inflammatory cell infiltration in sh-NC + MI/RI group. However, there was no myocardial necrosis and inflammatory cell infiltration in sh-circMIRIAF + MI/RI group. circMIRIAF shRNA reduced serum cTn-I and CK-MB levels in MI/RI mice (Fig. 6F). Serum cTn-I and CK-MB levels in sh-NC + MI/RI group were significantly increased compared with sh-NC group, which were decreased in sh-circMIRIAF + MI/RI group compared with sh-NC + MI/RI group ($P < 0.01$).

After circMIRIAF shRNA treatment, the level of circMIRIAF was decreased, and the level of miR-544 was increased in mice myocardium (Fig. 6G). The level of circMIRIAF was increased in sh-NC + MI/RI group compared with sh-NC group, and the level of circMIRIAF was decreased in sh-circMIRIAF + MI/RI group compared with sh-NC + MI/RI group. The level of miR-544 was decreased in sh-NC + MI/RI group compared with sh-NC group, which was increased in sh-circMIRIAF group. Further, miR-544 level was increased in sh-circMIRIAF + MI/RI group compared with sh-NC + MI/RI group, and there was no significant difference between sh-NC group and sh-circMIRIAF + MI/RI group (Fig. 6G). The mRNA levels of *IL-1β*, *IL-6*, *TNF-α*, *ICAM-1* were increased in sh-NC + MI/RI group compared with sh-NC group, which were decreased in sh-circMIRIAF + MI/RI group compared with sh-NC + MI/RI group (Fig. 6H). In addition, SOD level in myocardial tissue of sh-NC + MI/RI group was decreased compared with sh-NC group, and SOD level was decreased in sh-circMIRIAF + MI/RI groups compared with sh-NC + MI/RI group (Fig. 6I). The effects of circMIRIAF shRNA on protein levels in WDR12/Notch1 signal in mice are shown in Fig. 6J. After MI/RI, the level of WDR12 was up-regulated, and the levels of Notch1 and Activated Notch1 were down-regulated. However, the levels of WDR12, Notch1 and Activated Notch1 in sh-circMIRIAF + MI/RI groups were reversed by circMIRIAF shRNA. The levels of downstream proteins in Notch1 pathway were also changed accordingly. Based on the above tests, the results showed that circMIRIAF was negatively correlated with miR-544 (Correlation coefficient: −0.76), while circMIRIAF was positively correlated with WDR12 (Correlation coefficient: 0.87) (Fig. 6K). Thus, circMIRIAF regulated WDR12/Notch1 signal pathway by sponge adsorption of miR-544 to exacerbate MI/RI in mice.

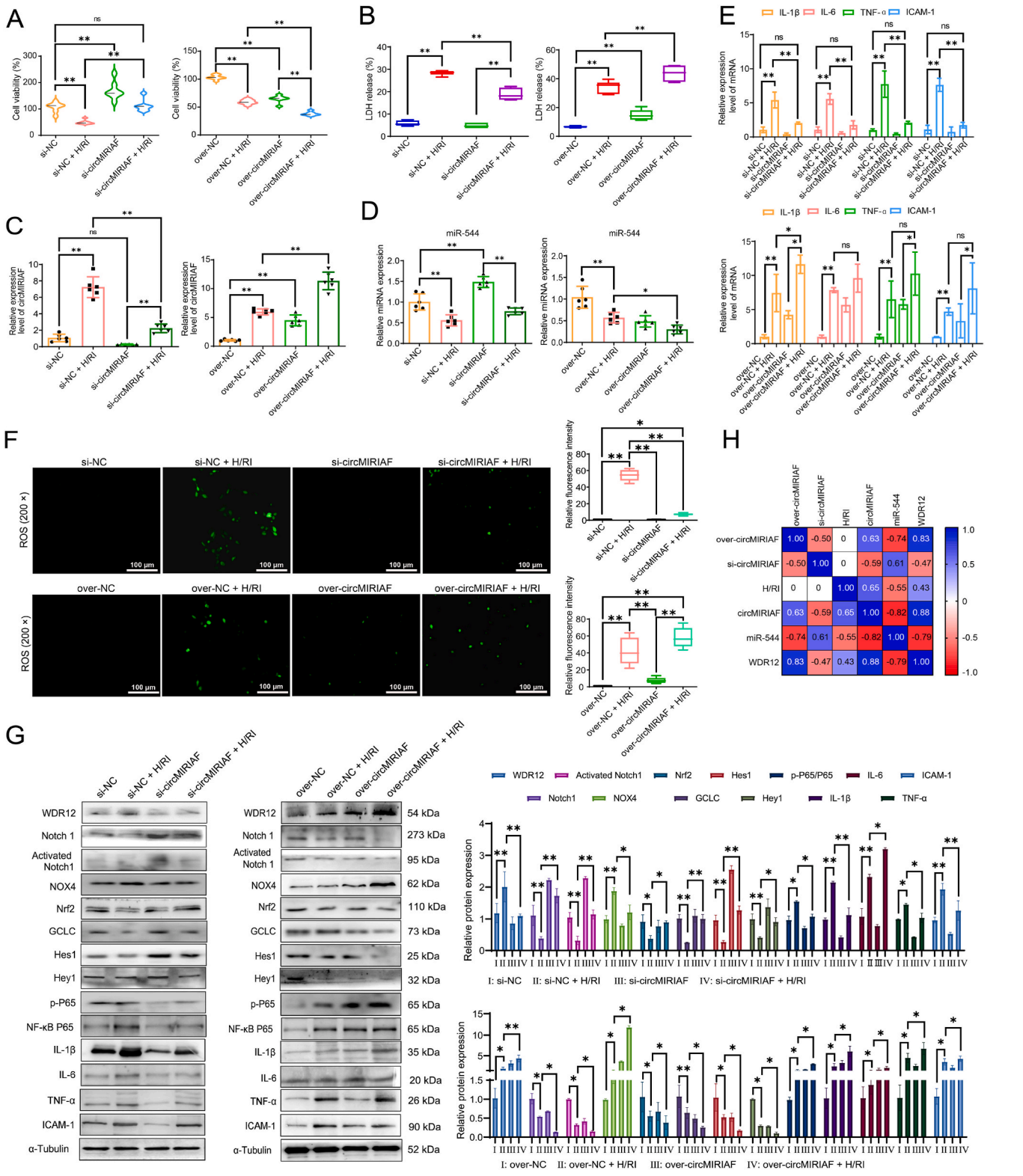

Fig. 5. circMIRIAF siRNA attenuates H/RI and circMIRIAF overexpression aggravates H/RI in AC16 cells. (**A**) The viability of AC16 cells transfected with circMIRIAF siRNA or circMIRIAF overexpression plasmid (n = 6). (**B**) The LDH release of AC16 cells transfected with circMIRIAF siRNA or circMIRIAF overexpression plasmid (n = 6). (**C**) The expression level of circMIRIAF in AC16 cells transfected with circMIRIAF siRNA or circMIRIAF overexpression plasmid (n = 6). (**D**) The expression level of miR-544 in AC16 cells transfected with circMIRIAF siRNA or circMIRIAF overexpression plasmid (n = 6). (**E**) The mRNA levels of intracellular *IL-1β*, *IL-6*, *TNF-α* and *ICAM-1* in AC16 cells transfected with circMIRIAF siRNA or circMIRIAF overexpression plasmid (n = 6). (**F**) The ROS level in AC16 cells transfected with circMIRIAF siRNA or circMIRIAF overexpression plasmid (n = 3). (**G**) The expression levels of WDR12, Notch1, Activated Notch1 and downstream proteins in AC16 cells transfected with circMIRIAF siRNA and circMIRIAF overexpression plasmid (n = 3). (H) Correlation analysis of circMIRIAF siRNA, circMIRIAF overexpression, H/RI with circMIRIAF, miR-544 and WDR12 expression. Data are shown as mean ± SD. *$P < 0.05$, **$P < 0.01$, *ns* is no significant difference.

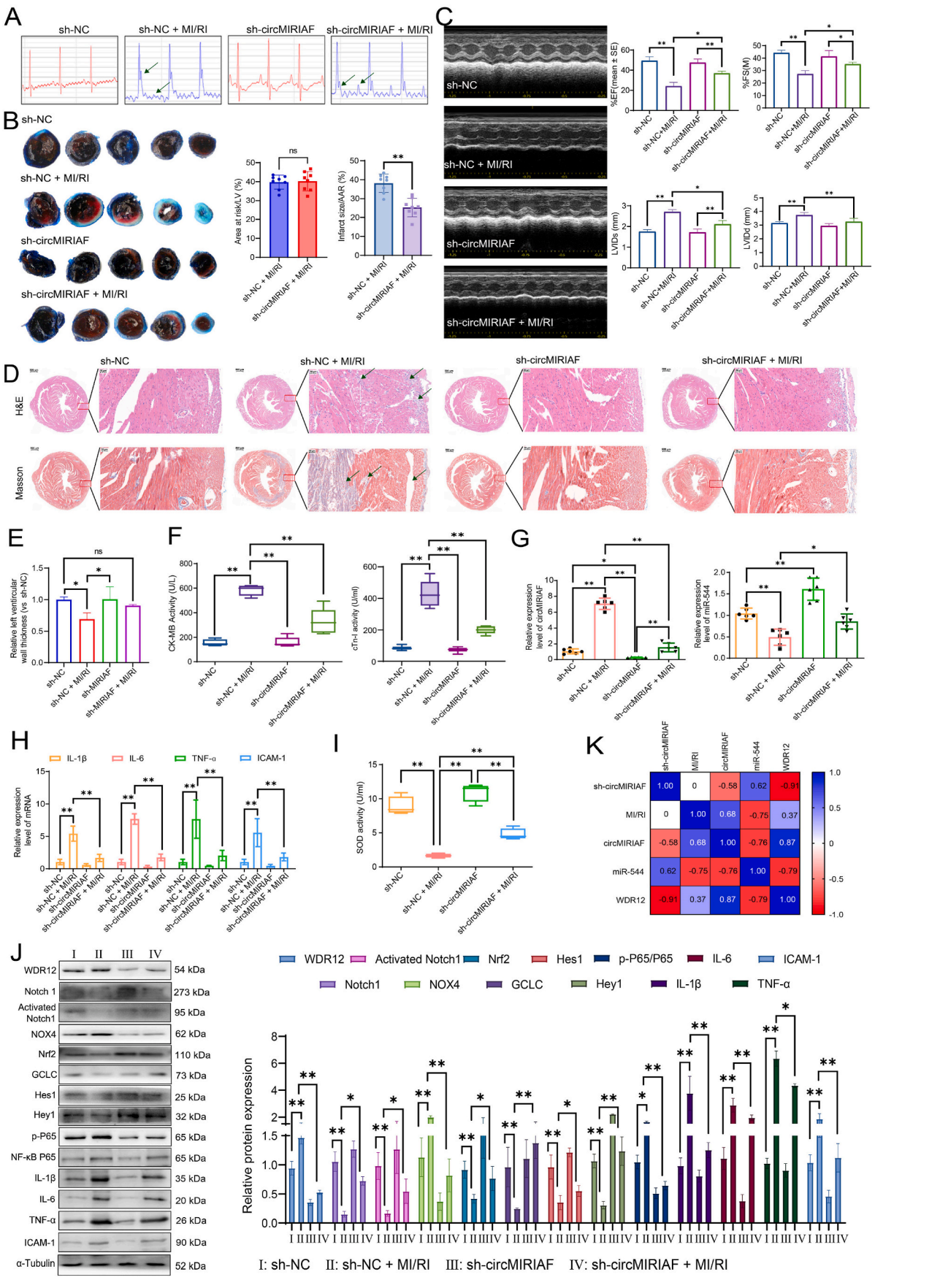

(caption on next page)

Fig. 6. circMIRIAF shRNA attenuates MI/RI in mice. (**A**) The ECG of mice transfected with circMIRIAF shRNA (n = 3). (**B**) Representative images of TTC/Evans blue staining of the hearts of mice transfected with circMIRIAF shRNA. The ratios of area at risk (AAR) to left ventricular area (LV) and infarct size normalized to AAR are shown (n = 8). (**C**) Echocardiography of hearts of mice transfected with circMIRIAF shRNA (n = 5). (**D**) H&E and Masson staining of myocardial tissue of mice transfected with circMIRIAF shRNA, scale bars = 500 μm and 50 μm (n = 3). (**E**) The relative left ventircular wall thickness of myocardial tissue of mice transfected with circMIRIAF shRNA (n = 3). (**F**) The serum CK-MB and cTn-I levels of MI/RI mice transfected with circMIRIAF shRNA (n = 6). (**G**) The expression levels of circMIRIAF and miR-544 of myocardial tissue of MI/RI mice transfected with circMIRIAF shRNA (n = 6). (**H**) The expression levels of *IL-1β*, *IL-6*, *TNF-α* and *ICAM-1* of myocardial tissue of MI/RI mice transfected with circMIRIAF shRNA (n = 6). (**I**) The SOD level of myocardial tissue of MI/RI mice transfected with circMIRIAF shRNA (n = 6). (**J**) The expression levels of WDR12, Notch1, Activated Notch1 and downstream proteins of myocardial tissue of MI/RI mice transfected with circMIRIAF shRNA (n = 3). (**K**) Correlation analysis of circMIRIAF shRNA, MI/RI with circMIRIAF, miR-544 and WDR12 expression. Data are shown as mean ± SD. $^{*}P < 0.05$, $^{**}P < 0.01$, *ns* is no significant difference.

3.8. circMIRIAF siRNA reverses WDR12 overexpression-induced H/RI aggravation in AC16 cells

WDR12 overexpression decreased cell viability and increased LDH release in over-WDR12 + H/RI group compared with over-WDR12 group (Fig. 7A). While, cell viability was increased and LDH release was decreased in si-circMIRIAF + over-WDR12 + H/RI group compared with over-WDR12 + H/RI group. And the data in Fig. 7B showed that the level of circMIRIAF was increased and the level of miR-544 was decreased after H/RI. While AC16 cells were treated by WDR12 overexpression plasmid, the mRNA level of WDR12 was increased. Further, the level of circMIRIAF was decreased in si-circMIRIAF + over-WDR12 + H/RI group compared with over-WDR12 + H/RI group. The level of miR-544 in si-circMIRIAF + over-WDR12 + H/RI group was increased compared with over-WDR12 + H/RI group, but there was no significant difference between over-WDR12 group and over-NC. The data in Fig. 7C showed that ROS levels in over-WDR12 group, over-NC + H/RI group and over-WDR12 + H/RI group were increased compared with over-NC group, which was decreased in si-circMIRIAF + over-WDR12 + H/RI group compared with over-WDR12 + H/RI group. Further, the mRNA level of *WDR12* was increased after H/RI. The levels of *WDR12* in over-NC + H/RI group and over-WDR12 groups were increased compared with over-NC group, which was increased in over-WDR12 + H/RI group compared with over-WDR12, and increased in si-circMIRIAF + over-WDR12 + H/RI group compared with over-WDR12 + H/RI group (Fig. 7D). Further validation of *IL-1β*, *IL-6*, *TNF-α* and *ICAM-1* mRNA levels was conducted (Fig. 7E). Thus, circMIRIAF showed a positive regulatory effect on WDR12 to regulate oxidative stress and inflammation in MI/RI mice though miR-544/WDR12 axis. The data in Fig. 7F showed the same trend of the protein levels in the signal pathway in over-WDR12 group, over-NC + H/RI group and over-WDR12 + H/RI group. WDR12 level was increased, and the levels of Notch1 and Activated Notch1 were decreased. The levels of NOX4, p-P65, IL-1β, IL-6, TNF-α and ICAM-1 were increased, and the levels of Nrf2, GCLC, Hes1 and Hey1 were decreased in over-WDR12 + H/RI group compared with over-NC + H/RI group. Thus, WDR12 exacerbated oxidative stress and inflammation caused by H/RI. While, the levels of those proteins were reversed by circMIRIAF siRNA in si-circMIRIAF + over-WDR12 + H/RI group. Based on the experiments, the results showed that circMIRIAF shRNA was negatively correlated with WDR12 (Correlation coefficient: −0.32), while WDR12 overexpression was positively correlated with WDR12 (Correlation coefficient: 0.79), and circMIRIAF was positively correlated with WDR12 (Correlation coefficient: 0.71) (Fig. 7G).

4. Discussion

At present, many researchers have carried on studies of therapeutic strategies to reduce myocardial injury, and circRNAs are confirmed as drug therapeutic targets [60]. For instance, circHIPK3 protects CMVECs under oxidative conditions [61], and circ-Ttc3 is significantly up-regulated in ischemic myocardium and hypoxic injured cardiomyocytes [62]. The roles of circRNAs in MI/RI are largely achieved through sponge adsorption of miRNAs. circ_Ddx60 inhibits apoptosis in myocardial cells by regulating miR-302a-3p/Bcl2a1a axis [63]. circ-NNT mediates MI/RI through activating pyroptosis by miR-33a-5p and regulating USP46 expression [64]. circRNA FEACR inhibits ferroptosis and alleviates MI/RI by interacting with NAMPT [65]. circ_0050908 up-regulates TRAF3 by sponging miR-324-5p to aggravate myocardial ischemia-reperfusion injury [66]. Although many studies on the roles of circRNAs in MI/RI have been reported, there are currently very few drugs via regulating circRNAs for clinical treatment. Therefore, it is necessary to explore critical circRNAs targets and develop innovative drugs for clinical prevention and treatment of MI/RI. Our study found that circMIRIAF played an important role in MI/RI, and silencing circMIRIAF effectively improved MI/RI. Therefore, circMIRIAF should be one drug target for efficient treatment of MI/RI.

Initially, we used human circRNA microarray screening analysis to discover circMIRIAF (circ_0006174) in H/RI AC16 cells. Further, RNA-seq technology was used to screen the differentially expressed mRNAs between H/RI group and normal group in AC16 cells. As a generation of sequencing technology, RNA-seq has great potential in solving disease problems [49]. The combination of human circRNA microarray screening analysis and RNA-seq can more efficiently and accurately predict the miRNAs adsorbed by circMIRIAF sponge. Centers on circMIRIAF, the miRNA with binding sites to circMIRIAF and differentially expressed mRNA were predicted by ceRNA analysis. Through the ceRNA analysis, we found that circMIRIAF should target WDR12 by sponge adsorption of miR-544 to regulate MI/RI. WDR12, the predicted target gene of miR-544, is a member of the protein family ending in tryptophan aspartate repeats (WD repeats domain 12). It is a WD40 repeat protein and plays a key role in ribosome biosynthesis, which is also an essential factor for processing of the 32S precursor ribosomal RNA [67]. Up-regulated WDR12 in heart failure is closely related to coronary heart disease, which can lead to deterioration of heart function [59,68], and *WDR12* gene polymorphisms are associated with nighttime ambulatory systolic-diastolic pressure regression index in hypertensive patients with cardiovascular disease [69]. In the present study, we found the increased levels of circMIRIAF, the decreased levels of miR-544 and the increased levels of WDR12 in MI/RI. Further, a binding site existed between circMIRIAF and miR-544 as well as miR-544 and WDR12, and circMIRIAF targeted WDR12 by sponge adsorption of miR-544 to regulate MI/RI. Therefore, circMIRIAF/miR-544/WDR12 was the target to explore the function and mechanism on regulating MI/RI.

In the study, we focus on finding drug targets closely related to oxidative stress and inflammation. MI/RI is an adverse reaction associated with the treatment of myocardial ischemia. Clinically, although drug thrombolysis and percutaneous coronary intervention are effective methods to reduce myocardial ischemia and improve the prognosis of patients, restoring blood flow yet will lead to myocardial reperfusion injury and further increase the infarct size of myocardium [12]. Oxidative stress and inflammatory response play important roles in MI/RI, which can increase intracellular Ca^{2+} and the destruction of mitochondrial membrane potential to cause ROS formation and inflammasomes [70,71]. Notch signaling pathway is involved in MI/RI to regulate oxidative stress and inflammation [72,73]. It has reported that WDR12 is a regulator of Notch signal [74]. Other studies have shown that Notchless encodes a novel WD40-repeat-containing protein to modulate Notch signaling activity, and WDR12 interacts with Notch1 to regulate the signal [75,76]. Our present study confirmed that WDR12 regulated oxidative stress and inflammation by regulating Notch1

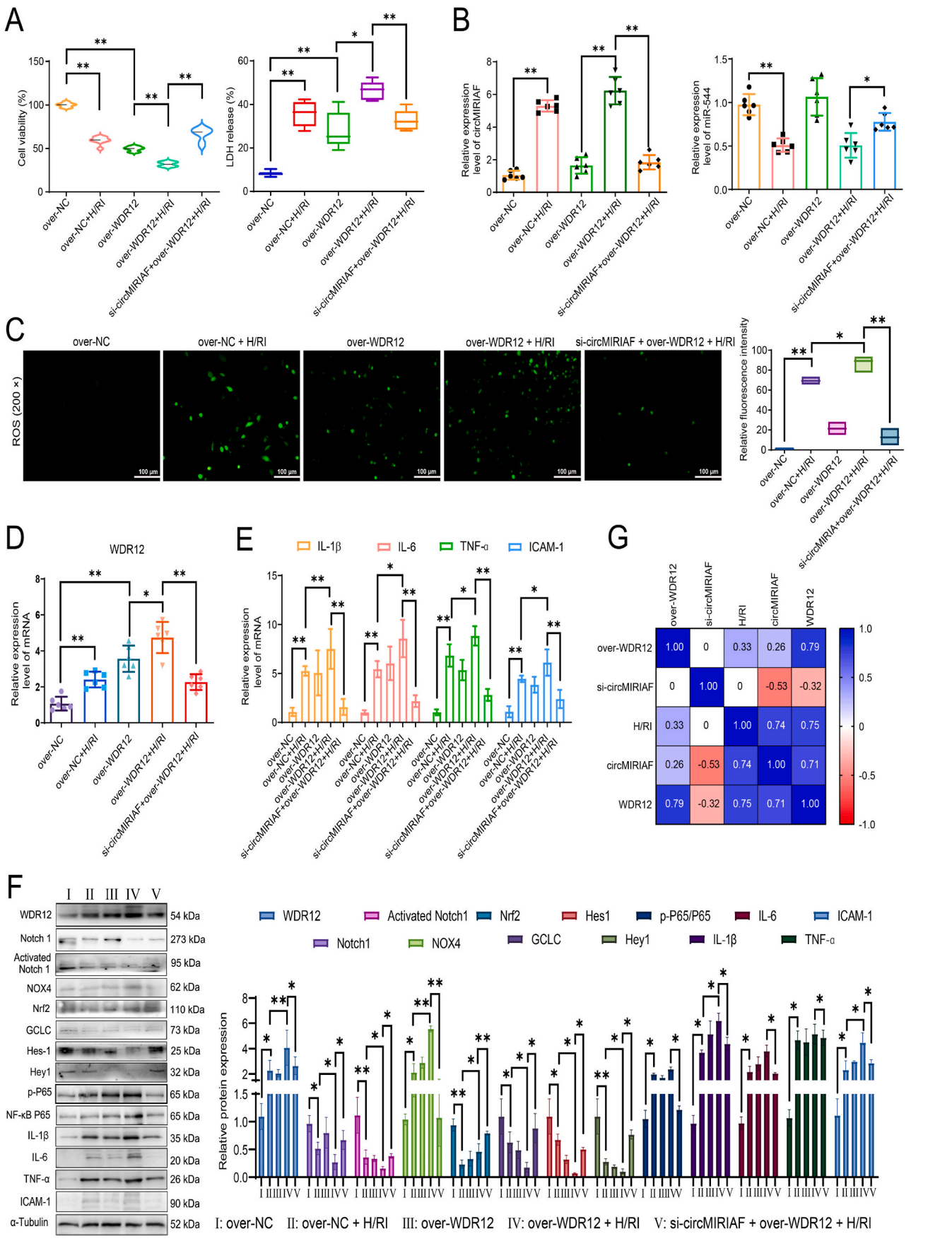

(caption on next page)

Fig. 7. circMIRIAF siRNA reverses WDR12 overexpression-induced H/RI aggravation in AC16 cells. (**A**) The cell viability and LDH release of AC16 cells transfected with circMIRIAF siRNA and WDR12 overexpression plasmid (n = 6). (**B**) The expression level of circMIRIAF and miR-544 in AC16 cells transfected with circMIRIAF siRNA and WDR12 overexpression plasmid (n = 6). (**C**) The ROS level in AC16 cells transfected with circMIRIAF siRNA and WDR12 overexpression plasmid (n = 3). (**D**) The expression level of *WDR12* in AC16 cells transfected with circMIRIAF siRNA and WDR12 overexpression plasmid (n = 6). (**E**) The mRNA levels of intracellular *IL-1β*, *IL-6*, *TNF-α* and *ICAM-1* in AC16 cells transfected with circMIRIAF siRNA and WDR12 overexpression plasmid (n = 6). (**F**) The expression levels of WDR12, Notch1, Activated Notch1 and downstream proteins in AC16 cells transfected with circMIRIAF siRNA and WDR12 overexpression plasmid (n = 3). (**G**) Correlation analysis of circMIRIAF shRNA, WDR12 overexpression, H/RI with circMIRIAF and WDR12 expression. Data are shown as mean ± SD. $^{*}P < 0.05$, $^{**}P < 0.01$.

signaling pathway in MI/RI. Overexpression of WDR12 in AC16 cells reduced Notch1 expression during H/RI, thereby exacerbating oxidative stress and inflammation. We also confirmed that circMIRIAF competitively adsorbed miR-544 to reduce the inhibition of miR-544 on WDR12 in MI/RI, namely, miR-544 inhibition induced MI/RI aggravation via WDR12/Notch1-mediated oxidative stress and inflammation, and circMIRIAF overexpression aggravated Notch1-mediated oxidative stress and inflammation through miR544/WDR12 axis. circMIRIAF inhibition attenuated Notch1-mediated oxidative stress and inflammation through miR-544/WDR12 axis, and circMIRIAF silencing ameliorated H/RI in AC16 cells induced by WDR12 overexpression.

There are still some limitations in the methods for verifying the relationship of circMIRIAF-miRNA and miRNA-mRNA, and a single dose of circMIRIAF siRNA or circMIRIAF shRNA was used in the present work. A better approach is to conduct research and statistical analysis on the relationship between the administrated concentration of circMIRIAF siRNA or circMIRAFA overexpression plasmids with the expression level of miR-544, which can more accurately illustrate the negative regulatory relationship between circMIRIAF and miR-544. The same limitations existed in the study of the relationship between miR-544 and WDR12. In the development of innovative drugs targeting circMIRIAF, it is necessary to ensure the integrity and accuracy of the relationship between compounds, circMIRIAF, miR-544, WDR12 and pharmacodynamics.

5. Conclusions

circMIRIAF played an important role in MI/RI to increase WDR12 expression by competitively sponging miR-544, thereby activating Notch1-mediated oxidative stress and inflammatory response to aggravate the disease. Modifying the binding site of circMIRIAF and developing drugs targeting specific circMIRIAF may change the expression level of downstream target genes to effectively treat MI/RI. The work on miR-544/WDR12/Notch1 signal may expose other potential therapeutic targets for MI/RI. The results of the present study provide a potential insight into the molecular mechanisms and therapeutic strategy for MI/RI.

CRediT authorship contribution statement

Lianhong Yin: Methodology, Investigation, Formal analysis, Validation, Writing – original draft. **Lili Li:** Investigation, Validation, Data curation, Formal analysis. **Meng Gao:** Conceptualization, Methodology, Visualization. **Yan Qi:** Formal analysis, Data curation, Software, Validation. **Lina Xu:** Conceptualization, Supervision, Visualization. **Jinyong Peng:** Conceptualization, Resources, Project administration, Writing – review & editing.

Declaration of competing interest

The authors declare that they have no known competing financial interests or personal relationships that could have appeared to influence the work reported in this paper.

Data availability

The data that has been used is confidential.

Appendix A. Supplementary data

Supplementary data to this article can be found online at https://doi.org/10.1016/j.redox.2024.103175.

References

[1] B.J. Gersh, K. Sliwa, B.M. Mayosi, S. Yusuf, Novel therapeutic concepts: the epidemic of cardiovascular disease in the developing world: global implications, Eur. Heart J. 31 (2010) 642–648.

[2] R. Mittal, V.M. Jhaveri, S.S. Kay, A. Greer, K.J. Sutherland, H.S. McMurry, N. Lin, J. Mittal, A.K. Malhotra, A.P. Patel, Recent advances in understanding the pathogenesis of cardiovascular diseases and development of treatment modalities, Cardiovasc. Hematol. Disord.: Drug Targets 19 (2019) 19–32.

[3] A.C. Passaroni, M.A. Silva, W.B. Yoshida, Cardiopulmonary bypass: development of John Gibbon's heart-lung machine, Rev. Bras. Cir. Cardiovasc. 30 (2015) 235–245.

[4] S. Reynolds, K. Waterhouse, K.H. Miller, Patient care after percutaneous transluminal coronary angioplasty, Nurs. Manag. 32 (2001), 51–54, 56.

[5] F.M. Khan, I. Hameed, M. Milojevic, M. Wingo, K. Krieger, L.N. Girardi, R. L. Prager, M. Gaudino, Quality metrics in coronary artery bypass grafting, Int. J. Surg. 65 (2019) 7–12.

[6] R.J. Shemin, The future of cardiovascular surgery, Circulation 133 (2016) 2712–2715.

[7] W. He, P. Chen, Q. Chen, Z. Cai, P. Zhang, Cytokine storm: behind the scenes of the collateral circulation after acute myocardial infarction, Inflamm. Res. 71 (2022) 1143–1158.

[8] H.I. Radwan, A.A.E. Ahmed, A.S. Ammar, H.S. Roshdy, Relation of collateral circulation with reciprocal changes in patients with acute ST-elevation myocardial infarction, J. Electrocardiol. 60 (2020) 36–43.

[9] A.T. Turer, J.A. Hill, Pathogenesis of myocardial ischemia-reperfusion injury and rationale for therapy, Am. J. Cardiol. 106 (2010) 360–368.

[10] D.J. Hausenloy, D.M. Yellon, Myocardial ischemia-reperfusion injury: a neglected therapeutic target, J. Clin. Invest. 123 (2013) 92–100.

[11] M. Neri, I. Riezzo, N. Pascale, C. Pomara, E. Turillazzi, Ischemia/reperfusion injury following acute myocardial infarction: a critical issue for clinicians and forensic pathologists, Mediat. Inflamm. 2017 (2017) 7018393.

[12] A. Frank, M. Bonney, S. Bonney, L. Weitzel, M. Koeppen, T. Eckle, Myocardial ischemia reperfusion injury: from basic science to clinical bedside, Semin. Cardiothorac. Vasc. Anesth. 16 (2012) 123–132.

[13] S. Toldo, A.G. Mauro, Z. Cutter, A. Abbate, Inflammasome, pyroptosis, and cytokines in myocardial ischemia-reperfusion injury, Am. J. Physiol. Heart Circ. Physiol. 315 (2018) H1553–H1568.

[14] S. Cadenas, ROS and redox signaling in myocardial ischemia-reperfusion injury and cardioprotection, Free Radic. Biol. Med. 117 (2018) 76–89.

[15] T. Zhao, W. Wu, L. Sui, Q. Huang, Y. Nan, J. Liu, K. Ai, Reactive oxygen species-based nanomaterials for the treatment of myocardial ischemia reperfusion injuries, Bioact. Mater. 7 (2021) 47–72.

[16] Q. Sun, H. Ma, J. Zhang, B. You, X. Gong, X. Zhou, J. Chen, G. Zhang, J. Huang, Q. Huang, Y. Yang, K. Ai, Y. Bai, A self-sustaining antioxidant strategy for effective treatment of myocardial infarction, Adv. Sci. 10 (2023) e2204999.

[17] R. Rodrigo, J.C. Prieto, R. Aguayo, C. Ramos, Á. Puentes, A. Gajardo, E. Panieri, C. Rojas-Solé, J. Lillo-Moya, L. Saso, Joint cardioprotective effect of vitamin C and other antioxidants against reperfusion injury in patients with acute myocardial infarction undergoing percutaneous coronary intervention, Molecules 26 (2021) 5702.

[18] D.R. Janero, Therapeutic potential of vitamin E against myocardial ischemic-reperfusion injury, Free Radic. Biol. Med. 10 (1991) 315–324.

[19] S.Y. Ren, P. Lin, J. Wang, H. Yu, T. Lv, L. Sun, G. Du, Circular RNAs: promising molecular biomarkers of human aging-related diseases via functioning as an miRNA sponge, Mol. Ther. Methods Clin. Dev. 18 (2020) 215–229.

[20] Q. Su, X.W. Lv, Revealing new landscape of cardiovascular disease through circular RNA-miRNA-mRNA axis, Genomics 112 (2020) 1680–1685.

[21] Z.Z. Liang, C. Guo, M.M. Zou, P. Meng, T.T. Zhang, circRNA-miRNA-mRNA regulatory network in human lung cancer: an update, Cancer Cell Int. 20 (2020) 173.

[22] Z.A. Cheng, C. Yu, S. Cui, H. Wang, H. Jin, C. Wang, B. Li, M. Qin, C. Yang, J. He, Q. Zuo, S. Wang, J. Liu, W. Ye, Y. Lv, F. Zhao, M. Yao, L. Jiang, W. Qin, circTP63 functions as a ceRNA to promote lung squamous cell carcinoma progression by upregulating FOXM1, Nat. Commun. 10 (2019) 3200.

[23] K. Wang, T.Y. Gan, N. Li, C.Y. Liu, L.Y. Zhou, J.N. Gao, C. Chen, K.W. Yan, M. Ponnusamy, Y.H. Zhang, P.F. Li, Circular RNA mediates cardiomyocyte death

via miRNA-dependent upregulation of MTP18 expression, Cell Death Differ. 24 (2017) 1111–1120.
[24] X.Q. Zhu, J. Ding, B.Y. Wang, J. Wang, M. Xu, Circular RNA DLGAP4 is down-regulated and negatively correlates with severity, inflammatory cytokine expression and pro-inflammatory gene miR-143 expression in acute ischemic stroke patients, Int. J. Clin. Exp. Pathol. 12 (2019) 941–948.
[25] M.Y. Li, W. Ding, M.A. Tariq, W.G. Chang, X.J. Zhang, W.H. Xu, L. Hou, Y.F. Wang, J.X. Wang, A circular transcript of *ncx1* gene mediates ischemic myocardial injury by targeting miR-133a-3p, Theranostics 8 (2018) 5855–5869.
[26] L. Zong, W. Wang, CircANXA2 promotes myocardial apoptosis in myocardial ischemia- reperfusion injury via inhibiting miRNA-133 expression, BioMed. Res. Int. 2020 (2020) 8590861.
[27] Y.F. Song, L. Zhao, B.C. Wang, J.J. Sun, J.L. Hu, X.L. Zhu, J. Zhao, D.K. Zheng, Z. W. Ge, The circular RNA TLK1 exacerbates myocardial ischemia/reperfusion injury via targeting miR-214/RIPK1 through TNF signaling pathway, Free Radical Bio. Med. 155 (2020) 69–80.
[28] L. An, Y. Zhong, J. Tan, Y. Liu, A. Li, T. Yang, S. Wang, Y. Liu, H. Gao, Sevoflurane exerts protection against myocardial ischemia-reperfusion injury and pyroptosis through the circular RNA PAN3/microRNA-29b-3p/stromal cell-derived factor 4 axis, Int. Immunopharmacol. 120 (2023) 110219.
[29] J. Liu, W. Dong, C. Gao, Y. Meng, Salvianolic acid B protects cardiomyocytes from ischemia/reperfusion injury by mediating circTRRAP/miR-214-3p/SOX6 axis, Int. Heart J. 63 (2022) 1176–1186.
[30] P. Jin, L.H. Li, Y. Shi, N.B. Hu, Salidroside inhibits apoptosis and autophagy of cardiomyocyte by regulation of circular RNA hsa_circ_0000064 in cardiac ischemia-reperfusion injury, Gene 767 (2021) 145075.
[31] R.A. Kovall, B. Gebelein, D. Sprinzak, R. Kopan, The canonical Notch signaling pathway: structural and biochemical insights into shape, sugar, and force, Dev. Cell 41 (2017) 228–241.
[32] M.E. Carlson, M.S. O'Connor, M. Hsu, I.M. Conboy, Notch signaling pathway and tissue engineering, Front. Biosci. 12 (2007) 5143–5156.
[33] Z.J. Zhang, D.F. Xu, S.N. Zhao, D. Lian, J. Wu, D.K. He, L. Li, Notch1 signaling pathway promotes proliferation and mediates differentiation direction in hippocampus of streptococcus pneumonia meningitis rats, J. Infect. Dis. 220 (2019) 1977–1988.
[34] P. Kratsios, C. Catela, E. Salimova, M. Huth, V. Berno, N. Rosenthal, F. Mourkioti, Distinct roles for cell-autonomous Notch signaling in cardiomyocytes of the embryonic and adult heart, Circ. Res. 106 (2010) 559–572.
[35] H.F. Pei, Q.J. Yu, Q. Xue, Y.P. Guo, L. Sun, Z.B. Hong, H. Han, E.H. Gao, Y. Qu, L. Tao, Notch1 cardioprotection in myocardial ischemia/reperfusion involves reduction of oxidative/nitrative stress, Basic Res. Cardiol. 108 (2013) 373.
[36] L. Yu, F. Li, G. Zhao, Y. Yang, Z. Jin, M. Zhai, W. Yu, L. Zhao, W. Chen, W. Duan, S. Yu, Protective effect of berberine against myocardial ischemia reperfusion injury: role of Notch1/Hes1-PTEN/Akt signaling, Apoptosis 20 (2015) 796–810.
[37] X.D. Li, F. Zou, Y.Y. Lu, X.P. Fan, Y.Y. Wu, X.L. Feng, X.Z. Sun, Y. Liu, Notch1 contributes to TNF-alpha-induced proliferation and migration of airway smooth muscle cells through regulation of the Hes1/PTEN axis, Int. Immunopharm. 88 (2020) 106911.
[38] W.Z. Jiao, J.F. Ji, F.J. Li, J.L. Guo, Y.J. Zheng, S.B. Li, W.W. Xu, Activation of the Notch-Nox4- reactive oxygen species signaling pathway induces cell death in high glucose-treated human retinal endothelial cells, Mol. Med. Rep. 19 (2019) 667–677.
[39] M. Yao, F. Gao, X.M. Wang, Y.M. Shi, S.X. Liu, H.J. Duan, Nox4 is involved in high glucose-induced apoptosis in renal tubular epithelial cells via Notch pathway, Mol. Med. Rep. 15 (2017) 4319–4325.
[40] S. Matsushima, J. Kuroda, T. Ago, P. Zhai, Y. Ikeda, S. Oka, G.H. Fong, R. Tian, J. Sadoshima, Broad suppression of NADPH oxidase activity exacerbates ischemia/reperfusion injury through inadvertent downregulation of hypoxia-inducible factor-1alpha and upregulation of peroxisome proliferator-activated receptor-alpha, Circ. Res. 112 (2013) 1135–1149.
[41] A.C. Brewer, T.V.A. Murray, M. Arno, M. Zhang, N.P. Anilkumar, G.E. Mann, A. M. Shah, Nox4 regulates Nrf2 and glutathione redox in cardiomyocytes in vivo, Free Radic. Biol. Med. 51 (2011) 205–215.
[42] Y. Jiang, C. Gu, H. Xu, F.Y. Shi, X.W. Zhang, F. Wang, iKeap1 activates Nrf2 signaling to protect myocardial cells from oxygen glucose deprivation/re-oxygenation-induced oxidative injury, Biochem. Biophys. Res. Commun. 574 (2021) 110–117.
[43] G. Boccalini, C. Sassoli, L. Formigli, D. Bani, S. Nistri, Relaxin protects cardiac muscle cells from hypoxia/reoxygenation injury: involvement of the Notch-1 pathway, Faseb. J. 29 (2015) 239–249.
[44] P. Zhu, M. Yang, H. He, Z. Kuang, M. Liang, A. Lin, S. Liang, Q. Wen, Z. Cheng, C. Sun, Curcumin attenuates hypoxia/reoxygenation-induced cardiomyocyte injury by downregulating Notch signaling, Mol. Med. Rep. 20 (2019) 1541–1550.
[45] D. Cao, S. Liu, M. Yang, K. Xie, Z. Zheng, H. Wen, X. Xie, Remifentanil preconditioning alleviates myocardial ischemia/reperfusion injury in rats via activating Jagged-1/Notch signaling pathway, Biosci. Rep. 10 (2021) BSR20210534.
[46] Z.Q. Huang, W. Xu, J.L. Wu, X. Lu, X.M. Chen, MicroRNA-374a protects against myocardial ischemia-reperfusion injury in mice by targeting the MAPK6 pathway, Life Sci. 232 (2019) 116619.
[47] R. Li, X. Qin, L. Yue, W. Liu, Y. Gao, F. Zhu, D. Wang, Q. Zhou, Nuciferine improves cardiac function in mice subjected to myocardial ischemia/reperfusion injury by upregulating PPAR-γ, Heliyon 9 (2023) e13630.
[48] X. Zhang, S. Wang, H. Wang, J. Cao, X. Huang, Z. Chen, P. Xu, G. Sun, J. Xu, J. Lv, Z. Xu, Circular RNA circNRIP1 acts as a microRNA-149-5p sponge to promote gastric cancer progression via the AKT1/mTOR pathway, Mol. Cancer 18 (2019) 20.
[49] W. Han, L. Wang, L. Zhang, Y. Wang, Y. Li, Circular RNA circ-RAD23B promotes cell growth and invasion by miR-593-3p/CCND2 and miR-653-5p/TIAM1 pathways in non-small cell lung cancer, Biochem. Biophys. Res. Commun. 510 (2019) 462–466.
[50] X. Lan, X. Liu, J. Sun, Q. Yuan, J. Li, CircRAD23B facilitates proliferation and invasion of esophageal cancer cells by sponging miR-5095, Biochem. Biophys. Res. Commun. 516 (2019) 357–364.
[51] J. Wei, Y. Lin, Z. Wang, Y. Liu, W. Guo, Circ_0006174 accelerates colorectal cancer progression through regulating miR-138-5p/MACC1 axis, Cancer Manag. Res. 13 (2021) 1673–1686.
[52] Y. Zhang, X. Tan, Y. Lu, Exosomal transfer of circ_0006174 contributes to the chemoresistance of doxorubicin in colorectal cancer by depending on the miR-1205/CCND2 axis, J. Physiol. Biochem. 78 (2021) 39–50.
[53] B. Huang, D.J. Cui, Y. Ren, X. Zhao, F. Li, W.Q. Yuan, Circ_0006174 promotes colorectal cancer progression by sponging microRNA-142-3p and regulating X-linked inhibitor of apoptosis expression, Int. J. Biol. Markers 36 (2021) 3–13.
[54] L. Yang, D.W. Ge, X. Chen, C.Z. Jiang, S.N. Zheng, miRNA-544a regulates the inflammation of spinal cord injury by inhibiting the expression of NEUROD4, Cell. Physiol. Biochem. 51 (2018) 1921–1931.
[55] Y. Yanaka, T. Muramatsu, H. Uetake, K. Kozaki, J. Inazawa, miR-544a induces epithelial-mesenchymal transition through the activation of WNT signaling pathway in gastric cancer, Carcinogenesis 36 (2015) 1363–1371.
[56] P.W. Lu, Y.T. Gu, L. Li, F. Wang, X.G. Qiu, miR-544a promotes breast cancer cell migration and invasion reducing cadherin 1 expression, Oncol. Res. 23 (2016) 165–170.
[57] T. Sun, Y. Liu, L. Liu, F. Ma, MicroRNA-544 attenuates diabetic renal injury via suppressing glomerulosclerosis and inflammation by targeting FASN, Gene 723 (2020) 143986.
[58] R. Fang, N.N. Zhao, K.X. Zeng, Q. Wen, P. Xiao, X. Luo, X.W. Liu, Y.L. Wang, MicroRNA-544 inhibits inflammatory response and cell apoptosis after cerebral ischemia reperfusion by targeting IRAK4, Eur. Rev. Med. Pharmacol. Sci. 22 (2018) 5605–5613.
[59] A.M. Moilanen, J. Rysä, L. Kaikkonen, T. Karvonen, E. Mustonen, R. Serpi, O. Tenhunen, Z. Bagyura, J. Näpänkangas, P. Ohukainen, P. Tavi, R. Kerkelä, M. Leósdóttir, B. Wahlstrand, T. Hedner, O. Melander, H. Ruskoaho, WDR12, a member of nucleolar PeBoW-complex, is up-regulated in failing hearts and causes deterioration of cardiac function, PLoS One 10 (2015) e0124907.
[60] L.L. Chen, L. Yang, Regulation of circRNA biogenesis, RNA Biol. 12 (2015) 381–388.
[61] H. Ni, W.F. Li, Y. Zhuge, S. Xu, Y. Wang, Y. Chen, G. Shen, F. Wang, Inhibition of circHIPK3 prevents angiotensin II-induced cardiac fibrosis by sponging miR-29b-3p, Int. J. Cardiol. 292 (2019) 188–196.
[62] L.D. Cai, B. Qi, X. Wu, S. Peng, G. Zhou, Y. Wei, J. Xu, S. Chen, S. Liu, Circular RNA Ttc3 regulates cardiac function after myocardial infarction by sponging miR-15b, J. Mol. Cell. Cardiol. 130 (2019) 10–22.
[63] Y. Sun, Y. Zhang, Z. Ye, Y. Wang, Y. Lao, J. Zhang, M. Fang, J. He, H. Yin, W. Yan, W. Jin, circRNA-miRNA complex participates in the apoptosis of myocardial cells in myocardial ischemia/reperfusion injury, Discov. Med. 33 (2022) 13–26.
[64] X. Ye, Y. Hang, Y. Lu, D. Li, F. Shen, P. Guan, J. Dong, L. Shi, W. Hu, CircRNA circ-NNT mediates myocardial ischemia/reperfusion injury through activating pyroptosis by sponging miR-33a-5p and regulating USP46 expression, Cell Death Dis. 7 (2021) 370.
[65] J. Ju, X.M. Li, X.M. Zhao, F.H. Li, S.C. Wang, K. Wang, R.F. Li, L.Y. Zhou, L. Liang, Y. Wang, Y.H. Zhang, K. Wang, Circular RNA FEACR inhibits ferroptosis and alleviates myocardial ischemia/reperfusion injury by interacting with NAMPT, J. Biomed. Sci. 30 (2023) 45.
[66] A. Jin, Q. Zhang, H. Cheng, C. Yang, X. Wang, Circ_0050908 up-regulates TRAF3 by sponging miR-324-5p to aggravate myocardial ischemia-reperfusion injury, Int. Immunopharm. 108 (2022) 108740.
[67] C.S. Ahn, H.K. Cho, D.H. Lee, H.J. Sim, S.G. Kim, H.S. Pai, Functional characterization of the ribosome biogenesis factors PES, BOP1, and WDR12 (PeBoW), and mechanisms of defective cell growth and proliferation caused by PeBoW deficiency in Arabidopsis, J. Exp. Bot. 67 (2016) 5217–5232.
[68] P. Blattmann, C. Schuberth, R. Pepperkok, H. Runz, RNAi-based functional profiling of loci from blood lipid genome-wide association studies identifies genes with cholesterol- regulatory function, PLoS Genet. 9 (2013) e1003338.
[69] M. Wirtwein, O. Melander, M. Sjögren, M. Hoffmann, K. Narkiewicz, M. Gruchala, W. Sobiczewski, Elevated ambulatory systolic-diastolic pressure regression index is genetically determined in hypertensive patients with coronary heart disease, Blood Pres. 26 (2017) 174–180.
[70] M.Y. Wu, G.T. Yiang, W.T. Liao, A.P. Tsai, Y.L. Cheng, P.W. Cheng, C.Y. Li, C.J. Li, Current mechanistic concepts in ischemia and reperfusion injury, Cell. Physiol. Biochem. 46 (2018) 1650–1667.
[71] M. Kawaguchi, M. Takahashi, T. Hata, Y. Kashima, F. Usui, H. Morimoto, A. Izawa, Y. Takahashi, J. Masumoto, J. Koyama, M. Hongo, T. Noda, J. Nakayama, J. Sagara, S. Taniguchi, U. Ikeda, Inflammasome activation of cardiac fibroblasts is essential for myocardial ischemia/reperfusion injury, Circulation 123 (2011) 594–604.
[72] L. Yu, H. Liang, Z. Lu, G. Zhao, M. Zhai, Y. Yang, J. Yang, D. Yi, W. Chen, X. Wang, W. Duan, Z. Jin, S. Yu, Membrane receptor-dependent Notch1/Hes1 activation by melatonin protects against myocardial ischemia-reperfusion injury: in vivo and in vitro studies, J. Pineal Res. 59 (2015) 420–433.

[73] L. Yu, F. Li, G. Zhao, Y. Yang, Z. Jin, M. Zhai, W. Yu, L. Zhao, W. Chen, W. Duan, S. Yu, Protective effect of berberine against myocardial ischemia reperfusion injury: role of Notch1/Hes1-PTEN/Akt signaling, Apoptosis 20 (2015) 796–810.
[74] B. Nal, E. Mohr, M.I. Silva, R. Tagett, C. Navarro, P. Carroll, D. Depetris, C. Verthuy, B.R. Jordan, P. Ferrier, Wdr12, a mouse gene encoding a novel WD-Repeat Protein with a notchless-like amino-terminal domain, Genomics 79 (2002) 77–86.
[75] R. Su, S.Y. Fu, Y.J. Zhang, R.J. Wang, Y.H. Zhou, J.Q. Li, W.G. Zhang, Comparative genomic approach reveals novel conserved microRNAs in Inner Mongolia cashmere goat skin and longissimus dorsi, Mol. Biol. Rep. 42 (2015) 989–995.
[76] J. Royet, T. Bouwmeester, S.M. Cohen, Notchless encodes a novel WD40-repeat-containing protein that modulates Notch signaling activity, EMBO J. 17 (1998) 7351–7360.